MECHANICAL CHARACTERIZATION OF POLYMER NANOCOMPOSITES AND THE ROLE OF INTERPHASE

A Thesis

Presented to the Academic Faculty

by

Daniel L. Ciprari

In Partial Fulfillment
Of the Requirements for the Degree
Master of Science in Materials Science and Engineering

Georgia Institute of Technology
November 2004

MECHANICAL CHARACTERIZATION OF POLYMER NANOCOMPOSITES AND THE ROLE OF INTERPHASE

Approved by:

Dr. Rina Tannenbaum, Chairperson
School of Materials Science & Engineering

Dr. Karl I. Jacob
School of Polymer, Textile & Fiber Engineering

Dr. Hamid Garmestani
School of Materials Science & Engineering

Date Approved: November 2004

DEDICATION

To my family, Kristen, Simon, and Luke, for continued love and support.

ACKNOWLEDGEMENT

I would like to thank my advisor, Dr. Rina Tannenbaum, for guidance, support, and wisdom through my graduate work. I would also like to thank Dr. Karl Jacob for his assistance in securing mechanical testing equipment and access to facilities. I would like to thank Rick Brown for tensile testing training, Dr. Chunming Jin for nanoindenter training, and Han Gi for DMA training. I would like to thank Will Hughes for his time and talent with gathering SEM images. I would like to acknowledge my group members through my time at Georgia Tech, Melissa Zubris, Jeremy Walker, Kasi David, Larry Pranger, and Erin Camponeschi who have contributed their time and expertise in assisting me with my research and have been both colleagues and friends. Finally, I would like to thank American Chemical Society Petroleum Research Fund (ACS PRF) and Air Force Office of Scientific Research (AFOSR) for providing funding for my research.

TABLE OF CONTENTS

LIST OF TABLES

LIST OF FIGURES

SUMMARY

Mechanical characterization of four polymer nanocomposite systems and two pure polymer reference systems was performed. Alumina (Al_2O_3) and magnetite (Fe_3O_4) nanoparticles were embedded in poly(methyl methacrylate) (PMMA) and polystyrene (PS) matrices. Mechanical testing techniques utilized include tensile testing, dynamic mechanical analysis (DMA), and nanoindentation. Consistent results from the three techniques proved that these nanocomposite systems exhibit worse mechanical properties than their respective pure polymer systems.

The interphase, an interfacial area between the nanoparticle filler and the polymer matrix, was investigated using two approaches to explain the mechanical testing results. The first approach utilized data from thermal gravimetric analysis (TGA) and scanning electron microscopy (SEM) to predict the structure and density of the interphase for the four nanocomposite systems. The second approach analyzed the bonding between the polymer and the nanoparticle surfaces using Fourier Transform Infrared Spectroscopy (FT-IR) to calculate the density of the interphase for the two PMMA-based nanocomposite systems. Results from the two approaches were compared to previous studies. The results indicate that Al_2O_3 nanoparticles are more reactive with the polymer matrix than are Fe_3O_4 nanoparticles, but neither have strong interaction with the polymer matrix. The poor interaction leads to low density interphase which results in the poor mechanical properties.

CHAPTER I

INTRODUCTION

A polymer composite is a combination of a polymer matrix and a strong reinforcing phase, or filler. Polymer composites provide desirable properties unavailable in matrix or filler materials alone.[1-4] A polymer nanocomposite is a polymer matrix with a reinforcing phase consisting of particles with one dimension in the nano-sized regime. In the past decade, extensive research has focused on polymer nanocomposites in hopes of exploiting the unique properties of materials in the nano-sized regime.[3-8] A general conclusion has been drawn that nanocomposites show much improved mechanical properties over their micro-sized similar systems.[3, 4, 6, 8-12] Because of their small size, nanoparticles have a high surface to volume ratio and provide high energy surfaces. An expected result of embedding nanoparticles into a polymer matrix is enhanced bonding between the polymer matrix and filler, resulting from the nanoparticles' high interfacial energy.[4, 6, 9, 13] Polymer composite theory predicts that improved bonding between polymer and matrix leads to improved mechanical properties.[4, 6, 9, 13, 14]

Despite these predictions, however, mechanical testing of nanocomposites has shown mixed results.[5, 15, 16] Some experimental data has shown that reduced particle size improves mechanical properties, specifically elastic modulus.[5, 6, 9] Other studies have shown that elastic modulus decreases with reduced dimensionality.[17] No clear conclusions have been made regarding trends in the mechanical properties of polymer nanocomposites.[4, 5, 15]

Although studies have focused on many different matrix-filler systems, a common feature of all polymer composites is the existence of a phase border between the matrix and filler and the formation of an interphase layer between them. The properties of the interphase can differ dramatically from the bulk and influence the mechanical properties of the composite. To explain the impact on properties, much theory has been applied to the study of interphase.[1, 5, 9, 12, 13, 16-21]

The focus of this research is to experimentally characterize mechanical properties of four polymer nanocomposite systems and investigate the role of interphase in their behavior. Alumina (Al_2O_3) nanoparticles and magnetite (Fe_3O_4) nanoparticles were each dispersed in polystyrene (PS) and poly(methyl methacrylate) (PMMA) matrices. Appropriate samples were created to support mechanical characterization using tensile testing, dynamic mechanical testing (DMA), and nanoindentation. Particle size and distribution were characterized using scanning electron microscopy (SEM) and transmission electron microscopy (TEM). Interphase bonding, density, and thickness were confirmed using Fourier transform infrared spectroscopy (FT-IR) and thermal gravimetric analysis (TGA).

Results from this study show a decrease in elastic modulus for these polymer nanocomposite systems. The limited ability of the polymer chains to strongly adhere to the nanoparticles produces interphase that is lower density than the bulk. These lower density regions coupled with the high number of nanoparticles needed to reach the 5% volume fraction chosen for this study degrade the mechanical properties of the nanocomposite.

CHAPTER II

BACKGROUND

Polymer systems are widely used because of their light weight, design flexibility, and processability.[7, 9] These systems, however, generally exhibit less attractive mechanical properties such as low strength and low elastic modulus as compared to metals and ceramics. One way to improve the mechanical properties of these systems while maintaining their desirable properties is by adding high-modulus reinforcing filler to make polymer composites.[2] Adding micro-sized inorganic filler particles to reinforce the polymeric materials has been standard practice in the composite industry for decades.[4, 11, 22, 23] Composite design efforts to achieve the optimal mechanical properties have focused on maximizing the interaction between the polymer matrix and the filler.[4-6, 9, 12, 14, 15, 22-26] Commonly, smaller fillers are used to increase the surface area available for interaction with the matrix.[4, 5, 8, 9, 11, 21, 23, 25, 26] However, in the case of micron sized fillers, content above 20% volume fraction is required to optimally impact mechanical properties. At these high concentrations the filler can detrimentally impact other benefits of polymers such as processability and appearance.[9]

With the advent of nanomaterials research, synthesis of inorganic nanoparticles, that is, particles with one dimension in the nano-sized regime, is readily achievable.[1, 5, 7, 8, 11, 12, 15, 25, 27] Because of their small size, nanoparticles have an extremely high surface to volume ratio providing significantly more surface area for bonding with the matrix than micro-sized fillers.[27] Polymer nanocomposites, consisting of a polymer matrix with

nanoparticle filler, have been predicted to be one of the most beneficial applications of nanotechnology. Much research has focused on the preparation and thermal and mechanical characterization of nanocomposites.[3, 4, 6-10, 17, 25, 28] Although some research has shown great improvement of mechanical properties from nanocomposites over those of micro-filled composites[5, 6, 9], results have not been consistent.[4, 5, 15, 17] Additionally, the varying polymer matrix/filler systems and varying preparation techniques do not support establishing clear trends in polymer nanoparticle performance.[15]

Current polymer models have not been able to consistently predict the properties of nanocomposites.[4, 5, 22, 29-31] Polymer composite theories in the past have relied on the idea that the modulus of a composite is a function of the mismatch of properties of constituents, volume fraction, shape and arrangement of inclusions, and matrix-inclusion interface.[4, 7, 9, 15] These theories, therefore, predict that the effect on the composite system is independent of the size of the inclusion. Recent theories have included the size of the filler particulate to predict the properties of composites.[6, 8, 9, 13, 15, 21, 23, 25, 31-33]

Interphase Review

An area of polymer composite structure that has always garnered attention is the region directly near the interface of the polymer matrix and the filler.[1, 5, 9, 12, 13, 16, 18, 24, 25] Despite the huge variety of polymer composite systems, a common thread among all the systems is the existence of a phase border between the matrix and filler and the formation of an interphase layer between them.[1, 2, 9, 13, 24] As seen in Figure 1, the interphase layer extends well beyond the adsorption layer of the matrix chains bound to the filler surface. The structure of the interphase is different than either the filler or matrix phases, and it varies depending on the distance from the bound surface.

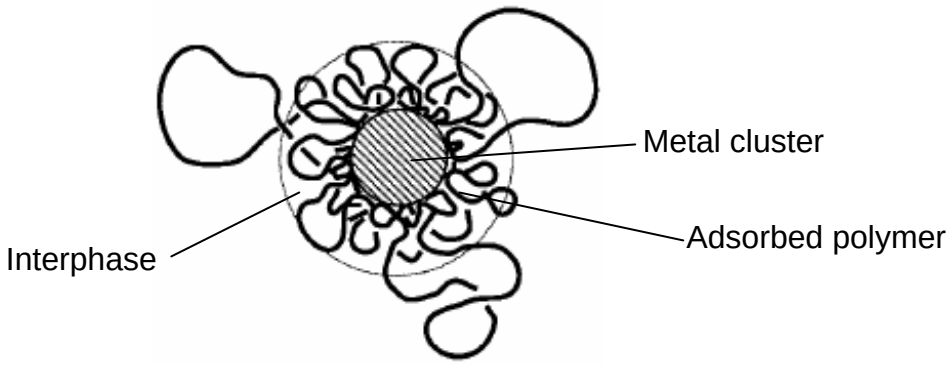

Figure 1. Schematic of interphase area between a filler and the polymer matrix.[33]

Because of the differences in structure, interphase properties can differ dramatically from the bulk polymer.[1, 9, 21, 24] The interphase is important to the mechanical properties of the composite because its distinct properties control the load transfer between matrix and filler.[1, 17, 22, 24, 25] The concept of interphase is not unique to

nanocomposites, but due to the large surface area of nanoparticles, the interphase can easily dominate the properties of nanocomposites.[9, 21, 24] An interphase 1 nm thick on microparticles in a composite represents as little as 0.3% of the total composite volume. However, an interphase 1 nm thick on nanoparticles can reach 30% of the total volume.[9] As shown in Figure 1, the interphase has a characteristic structure consisting of flexible polymer chains, typically in sequences of adsorbed segments (trains), loops, and tails. Interphase thickness is not a constant value because the interphase has no defined border with the bulk polymer.[2] The effective value of the thickness depends on chain flexibility and on the energy of adsorption, which is determined by the surface energies of the polymer and the solid. Because of conformational limitations brought by surface and statistical conformations of the polymer's coils in solutions, a relatively small number of segments are bound to the surface.[2] If all areas of the surface are capable of adsorption, the polymer chain is sufficiently flexible, and segments are readily adsorbed, the loops will be short and the macromolecule will form a flat (ie dense) layer close to the surface, as shown in Figure 2(a). If the chain segments have weak interaction with the surface, or the chain is rigid, the loops and tails extend farther into the matrix and form a region of lower density, as shown in Figure 2(b).[1]

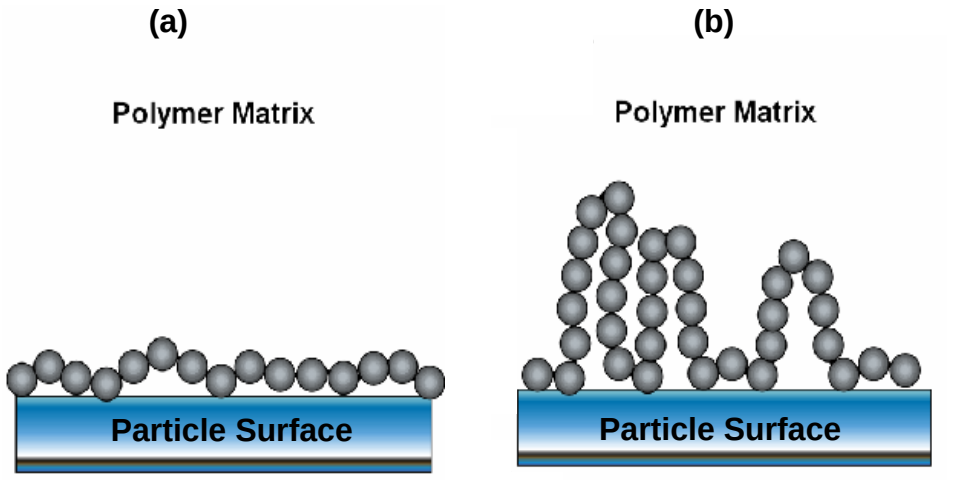

Figure 2. Schematic representation of a metal-polymer nanocomposite and adsorption characteristics on the surface of the metal oxide clusters in which (a) a strongly-binding polymer adheres to the surface and most of the segments reside on the surface, and a (b) weakly-binding polymer adheres to the surface and most of the segments reside in loops.[1]

The concept of an interphase is now widely accepted, although the influence of the interphase on the properties of a polymer composite has not yet been quantitatively established.[2, 6, 9, 17] Many studies have identified the interphase as an important factor in the mechanical properties of composites.[5, 6, 8, 9, 12] Vollenberg and Heiken proposed the role of interphase in their results, but their concepts are different than that proposed in the current study.[5] They explained an increase in modulus, yield, and tensile strength in composite systems by defining the properties of the interphase region. According to their theory, if a polymer adhered to a filler particle surface where modulus is high, there would be an area of high density, and thus, high modulus next to the particle. The polymer portion in the area just outside the particle will move toward the high density area, leaving an area of low density and low modulus just away from the high density

area. Vollenberg and Heiken proposed that for large particles, the size of the low density area will be relatively large which will lessen the impact of the higher modulus filler. But in a nanocomposite there are many more particles required to achieve the same volume fraction, so the particles are much closer together to achieve. If the particles are close enough the higher density bounded layer of the polymer will comprise a larger fraction of the matrix so the lower modulus will have little effect on the system.[5] This logic suggests that nanocomposites will have improved mechanical properties over large scale composites.

Nanocomposite Characterization Review

While there has been a great amount of experimental work that has taken place in the area of polymer nanocomposites, a consensus has not yet been reached on how nano-sized inclusions affect mechanical properties.[4, 15] Several studies have shown that reduced size improves mechanical properties, specifically elastic modulus.[5, 6, 8, 9] These studies vary in polymer nanocomposite systems and the mechanical properties characterized. The studies propose various theories to explain their results. The following section reviews the research and results.

Chan, et al. embedded calcium carbonate ($CaCo_3$) nanoparticles in a polypropylene (PP) matrix to study the nucleation effect of the nanoparticles and their impact on mechanical properties of the nanocomposite. The study dispersed the nanoparticles via melt mixing and achieved average particle size of 44 nm. Good dispersion of particles was achieved at 4.8% and 9.2% volume fractions, but many

aggregates were found at 13.2%. Nano-sized $CaCo_3$ inclusions in PP resulted in an 85% increase in modulus over the pure PP matrix. Micron-sized $CaCO_3$ inclusions in the matrix, however, showed little improvement in mechanical properties.[6] As shown in Figure 3, the improved modulus increases with volume fraction, the yield stress and tensile strength decrease with increased volume fraction, while the ultimate strain does not change with volume fraction.

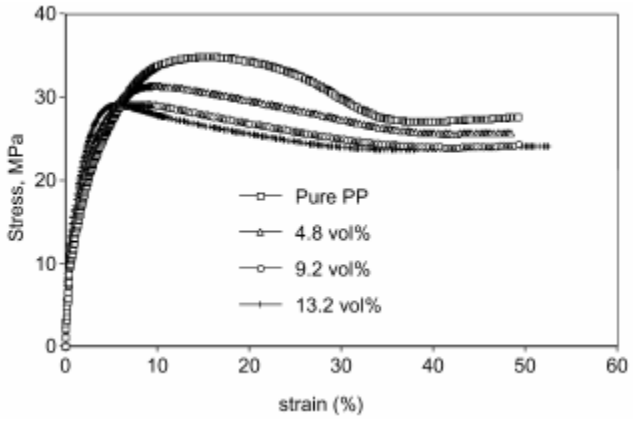

Figure 3. Stress-strain curves of the PP nanocomposite system.[6]

The authors of this study assumed the increase in modulus was due to a strong interaction between the polymer and filler, caused by the large interfacial area between them, resulting in reinforcing and nucleating effects by the $CaCo_3$ nanoparticles.[6] They proposed that the strong interaction and nucleation effects have a counter-balancing force on the mechanical properties. Strong interaction increases the yield strength and tensile strength but decreases the ultimate strain. But the strong nucleating effect reduces the size of the spherulites which has the opposite effect, decreasing the yield strength and tensile strength but increasing the ultimate strain. They propose the dispersion of

nanoparticles is critical as shown by the large impact on mechanical properties of the lower volume percent samples, in which they confirmed better dispersion.[6]

Shelley, et al. showed that in a nylon-6 system with 5% weight fraction clay platelets, modulus increases 200%, yield strength increases 175%, and ultimate strain slightly decreases.[10] The same system with a lower weight fraction showed lower increases in modulus and yield strength but showed a slight increase in ultimate strain. The platelets had a surface area of 100 nm^2 with a thickness of 1 nm and were found to have good interaction with the matrix.[10]

In a different study, silica nanoparticles of 17, 30, and 80 nm size were embedded in a polyamide-6 matrix.[8] The elastic modulus was higher for the nanocomposites than for the pure system but showed little variation with particle size. Consistent with the polyamide system presented above, the yield stress increased with increasing filler concentration and increased slightly as the size of the particles decreased. Ultimate strain decreased greatly, however, as concentration increased and particle size decreased. The study observed a filler size effect on the filler dispersion and suggests a possible existence of an optimal size for the reinforcing particles.[8] The debonding process was examined to explain the differences in the mechanical properties between the particle sizes as shown in Figure 4. The study suggests that the 12 nm particles tend to gather into aggregates and a multiple debonding process results from debonding around each individual particle. The aggregates, therefore, act like large soft particles during the deformation process. The 50 nm particles are well distributed, however, and would preferentially undergo a single debonding process. The debonding theory was also used

to explain why the volume of the polymer nanocomposites increased, with the greatest increase occurring in systems with the smallest particles.

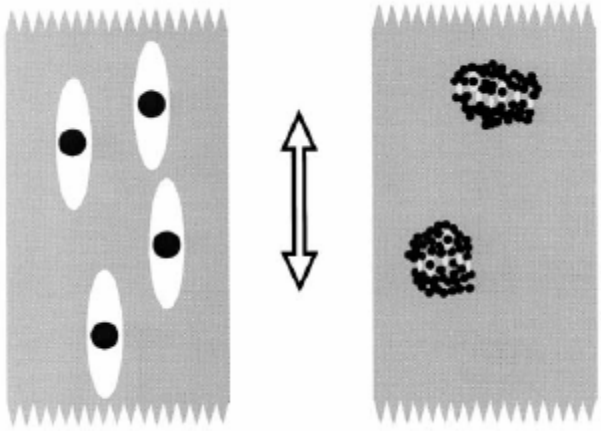

Figure 4. Schematic representations of the debonding process around 50 nm (left) and 12 nm (right) particles.[8]

Other research has shown that elastic modulus decreases or changes inconsistently with reduced dimensionality.[17, 21] Petrovic, et al. directly compared the mechanical properties of polyurethane-based composites formed using nano-size (10-20 nm) silica fillers against the properties of the composites formed using micron-size (1.4 μm) fillers. The study provided mixed results.[21] Mechanical and structural properties were examined as a function of filler concentration, 10-50% weight fraction. Samples with nanoparticles showed lower modulus than samples with microparticles at less than 40% weight fraction, but higher modulus at 40% and 50% weight fraction. Both nanosilica-filled and microsilica-filled composites showed increase in elastic modulus with increasing filler concentration in the glassy and rubber states but the change was less predictable in the nanocomposites. The tensile strength increased for nanocomposites but decreased for

microcomposites above 20% weight fraction, but varied little between the micron and nano-sized particles below 20% weight fraction. Ultimate strain increased 600% with nanofiller but increased only slightly with microfiller. Glass transition temperatures, T_g, were inconsistent across measurement methods. DSC showed no dependence on filler concentration or filler type. However, TMA, DTMA, and DEA showed T_g increased with increasing filler concentration for both nano and micron fillers, but showed a slightly higher increase with nanofillers. This study also observed a decrease in composite density, that is, an increase in volume, with nanofillers as compared to micron fillers. The study proposed that the results stemmed from chemical/physical interactions between the filler and the matrix and geometric constraints imposed by the close proximity of the filler particles.[21]

In this same study, Petrovic, et al. investigated the impact of nanoparticle fillers on composite hardness. Hardness is an important property for characterizing elastomers. Hardness increased consistently with microsilica across all concentrations. Hardness increased only slightly for nanosilica on low concentrations then decreased at higher concentrations. Interestingly, other studies have shown an increase in hardness with the addition of nanoparticles.[21]

Ash, et al. performed mechanical and thermal characterization of PMMA-alumina nanocomposites with 40 nm particles of varying concentration from 0 to 10 weight fraction.[17] The nanocomposites in this study were synthesized via free radical polymerization. The elastic modulus for all nanocomposite concentrations were lower than for pure PMMA. At the lowest filler content, there was a sharp initial drop in elastic modulus followed by a steady increase as concentration increased, but never reaching the

level of the pure system. In addition, the strain-to-failure for 5% weight fraction increased by around 800% over the pure system. However, the ultimate stress of the pure system was higher than for the composite as shown in Figure 5.[17]

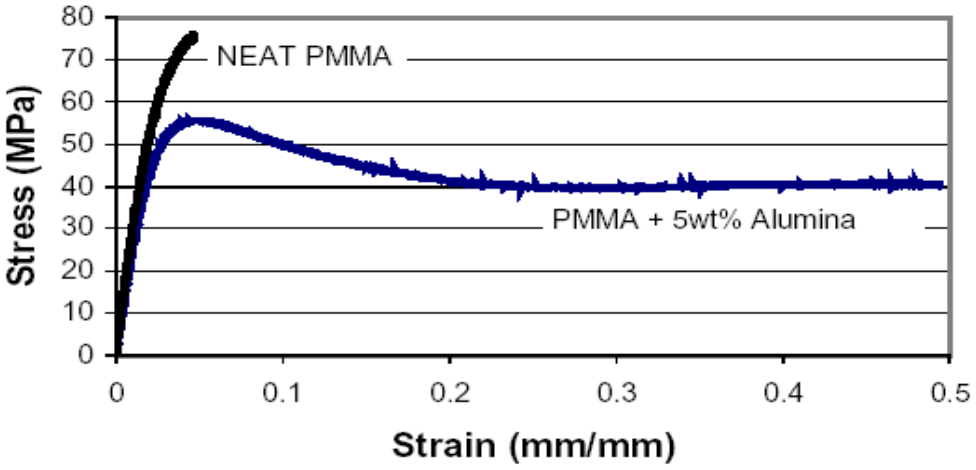

Figure 5. Stress strain curve for PMMA and alumina.[17]

In this study T_g decreased ~20˚C for the composites systems as compared to the pure system. The researcher related this decrease in T_g to that observed in thin films as a function of film thickness and interfacial properties in which higher chain mobility at the interfaces results in lower T_g. If the polymer were not bound to the particles, a matrix with many voids would result in very high interfacial area. A system of this type has the characteristics of a thin polymer film with a large surface to volume ratio.[17]

Analysis of SEM images of the fracture surfaces showed good dispersion of particles (Figure 6) and suggested a different fracture mechanism between the pure and nanocomposite systems. The pure surfaces show crazing that leads to brittle fracture. The fracture surface of the nanocomposites does not show attributes of crazing,

suggesting that the mode of failure has been altered from crazing to homogeneous yield. The study proposes that minimal bonding exists between the nanoparticles and the surrounding system, allowing voids surrounding the nanoparticles to expand, which prevents crazing.[17]

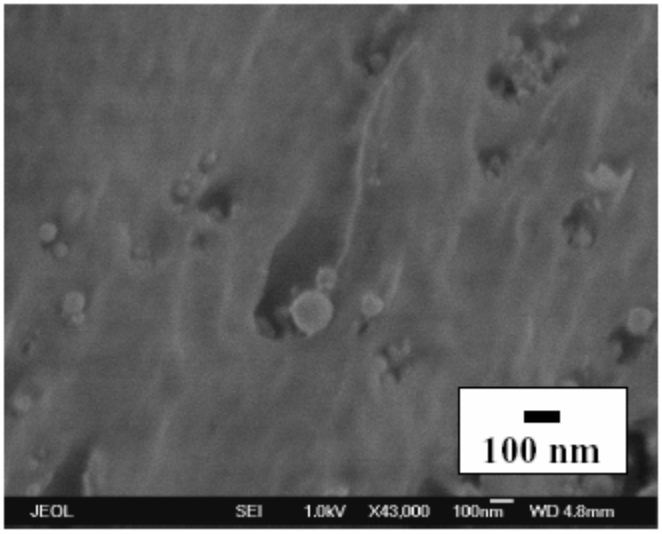

Figure 6. Fracture surface of PMMA nanocomposite containing uncoated alumina particles at 5% weight fraction.[17]

Nanoparticle Dispersion

A critical factor in nanocomposite properties is the dispersion of the nanoparticles in the polymer matrix.[5, 6, 8, 17, 25, 34] Dispersion of an inorganic nanoparticle filler in a thermoplastic is not easily achieved because nanoparticles have a strong tendency to agglomerate to reduce their surface energy.[5, 6, 25] Rong, et al. used grafting polymers to surround nanoparticles and produce better dispersion. Some studies have used adsorbed polymers to sterically stabilize nanoparticle dispersions limiting formation of flocculants

and aggregates.[1, 27, 34, 35] Other studies have used different approaches to in-situ polymerization to achieve good particle dispersion.[8, 15, 17, 36-38] Although the studies presented above utilized a wide range of sample preparation techniques, no technique proved significantly better than any others.[15]

Our Systems

During this study six systems were examined including four polymer nanocomposite systems and two reference systems: poly(methyl methacrylate) (PMMA, pure/reference), PMMA-Fe_3O_4, PMMA-Al_2O_3, polystyrene (PS, pure/reference), PS-Fe_3O_4, and PS-Al_2O_3. The goal in selecting the systems was to vary sizes of nanoparticles with similar reactivity and vary polymer matrix reactivity. Alumina (39 nm) nanoparticles and magnetite (90 nm) were chosen based on availability and size distribution as well as the existence of studies for comparing results.[17, 39]

PMMA and PS were chosen as the matrix materials based on their contrasting reactivity with metal oxides. Previous studies have shown PMMA adsorbs strongly to metal oxide nanoparticles through coordination of the carbonyl functional group to the metal surface sites. PS adsorbs weakly through dipole-dipole interactions between the π-electrons of the pendant benzene ring and the metal surface sites.[34] High molecular weight polymers with $\overline{M}_w$ =350,000 g/mol were chosen to maximize chain flexibility which provides the best potential for chain adherence to a nanoparticle surface.[1, 2] Filler volume fraction of 5% was chosen for all systems because it offers more opportunities for comparison to other studies.[5, 6, 17] In order to provide good solvents for the polymers,

chlorobenzene was chosen for the PMMA systems and Toluene was chosen for all PS systems.

Mechanical Characterization Techniques

Tensile Testing

Tensile testing was performed to determine elastic modulus, ultimate stress, and ultimate strain for all six systems. In tensile testing, a "dog-bone" shaped sample is placed in the grips of movable and stationary fixtures in a screw driven device, as shown in Figure 7, which pulls the sample until it breaks and measures applied load versus elongation of the sample.

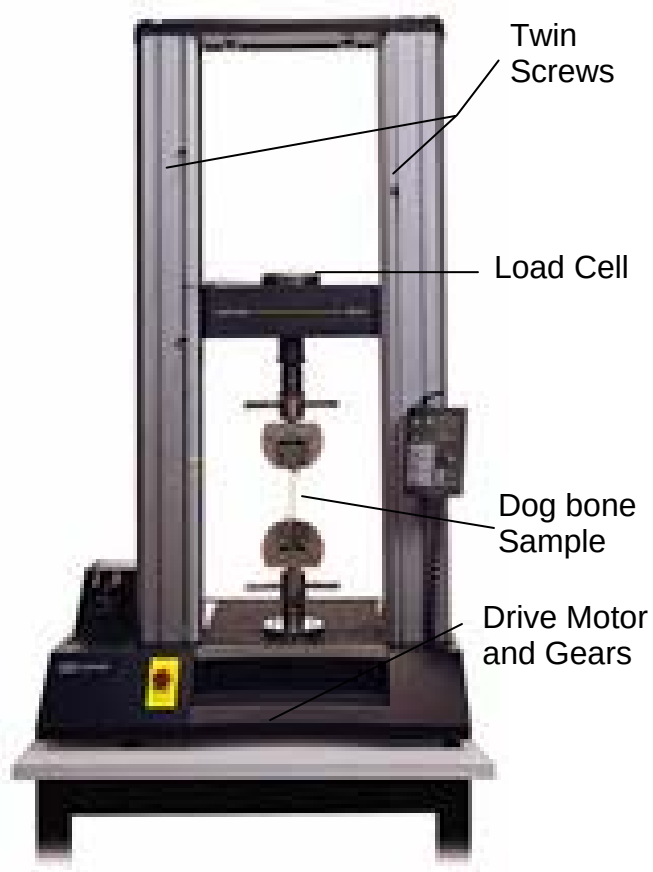

Figure 7. Tensile testing equipment.

The testing process requires specific grips, load cell, and extensometer for each material and sample type. The load cell is a finely calibrated transducer that provides a precise measurement of the load applied. The extensometer is calibrated to measure the smallest elongations. Output from the device is recorded in a text file including load and elongation data. Elongation is typically measured by the extensometer in volts and must be convserted to millimeters. Mechanical properties are determined from a stress vs. strain plot of the load and elongation data. Tensile testing is a destructive characterization technique. The American Society for Testing and Materials (ASTM) provides the following relevant standard test methods:

- D638 – Tensile Properties of Plastics
- D3039 – Tensile Properties of Polymer Matrix Composite Materials

Dynamic Mechanical Analysis

Dynamic mechanical analysis (DMA) was used to gather elastic modulus data for all six systems. DMA determines elastic modulus, loss modulus, and damping coefficient as a function of temperature, frequency, or time. The approach is often used to determine glass transition temperature, as well. Samples in DMA, depending on the equipment, can be quite small, in the range of 40 mm X 5 mm X 1 mm. The sample is clamped into movable and stationary fixtures and then enclosed in a thermal chamber, as shown in Figure 8.

Figure 8. A typical dynamic mechanical analysis system.[40]

The DMA applies torsional oscillation to the sample while slowly moving through the specified temperature range. Experimental nputs into the equipment include

frequency and amplitude of oscillations, static initial applied load, and temperature range. Results are typically recorded as a graphical plot of elastic modulus, loss modulus, and damping coefficient versus temperature. DMA, like tensile testing, is a destructive technique. The American Society for Testing and Materials (ASTM) provides the following relevant standard test methods:

- D4065 – Dynamic Mechanical Properties: Determination and Report of Procedures
- D4092-Terminology Related to Dynamic Mechanical Measurements on Plastics

Nanoindentation

Nanoindentation was used as another approach to gather comparative elastic modulus and hardness data for the six systems. The basic concept of indentation testing involves touching a material whose mechanical properties are of interest with a material whose properties are known. Nanoindentation is a specialized indentation test in which the penetration distance is measured in nanometers. Because the sample surface area and depth requirements are so small, thin film samples are appropriate for this type of testing. One of the key factors in analyzing indentation data is the contact area between the indenter and specimen. In typical indentation testing the area of contact is simply calculated from measurements of the residual impression left on the specimen. With nanoindentation, however, the area is on the order of microns and is too small to measure accurately.[41-43] Instead, the depth of penetration into the specimen surface is measured and combined with the known geometry of the indenter to calculate the contact area. The load displacement data gathered during the indentation process, shown in Figure 9, provides the means to calculate modulus and hardness.

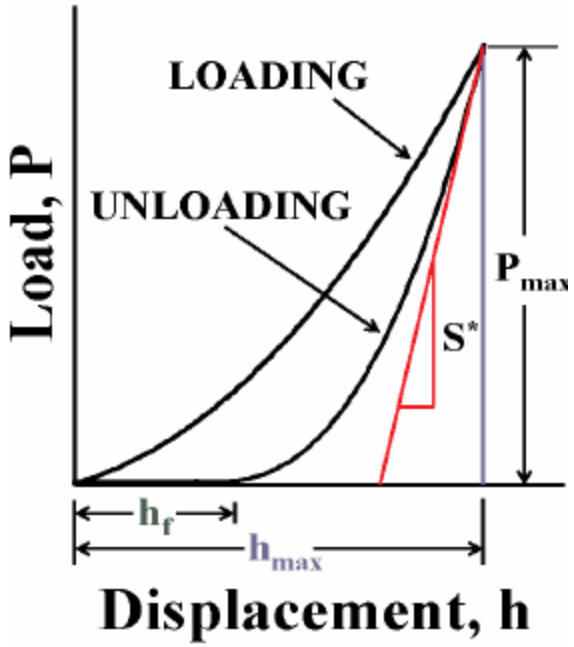

Figure 9. A typical indentation force-displacement curve. Pmax and hmax are the maximum load and displacement, respectively. S* is the slope of the tangent to the maximum load on the unloading curve.[44]

The maximum indenter depth achieved for a particular load and the slope of the unloading curve measured at the tangent to the data point at maximum load is used to calculate hardness and modulus following the method developed by Oliver and Pharr.[41]

Under indentation loading, creep within a specimen can occur and results in a change of indentation depth with a constant test force applied. It is indistinguishable from thermal drift so one must interpret results accordingly. Several studies performing nanoindentation on polymers, including specifically PS and PMMA, have shown larger modulus values than reported by tensile testing or DMA on the same materials.[41] The values of modulus tend to increase with indentation depth. Although the values might be larger than other characterization techniques, this study assumes nanoindentation can

provide sound comparative data as all six systems in this study were analyzed using the same parameters. Unlike tensile testing and DMA, nanoindentation is generally considered a non-destructive technique.[41] The American Society for Testing and Materials (ASTM) Task Group E28.06.11 is developing a standard test method for indentation testing.

Analytical Techniques

Thermal Gravimetric Analysis

Thermal gravimetric analysis (TGA) was used to determine the changes in polymer decomposition temperatures between the six samples and to help determine the thickness of the polymer layer surrounding the nanoparticles. TGA continuously measures the weight of a sample as a function of temperature and time. The sample is placed in a pan held in a microbalance. The pan and sample are heated in a controlled manner and weight is measured throughout the heating cycle. Changes in weight at specific temperatures correspond to reaction or changes in the sample such as decomposition.[45] The weight loss experienced during the decomposition experiment corresponds to the amount of polymer that was attached to the particles in the sample.

Transmission Electron Microscopy

Transmission electron microscopy (TEM) was used to characterize the size of the particles present in the four nanocomposite systems. TEM enables the visualization of internal structure of crystal samples and provides two dimensional images magnified as

high as 100,000 times by use of transmitted electrons. Because electrons can only travel a short distance through matter, samples must be very thin to enable acceptable image resolution. Samples are prepared on a wire mesh TEM grid, with ideal specimen thickness less than 100 nm. Observing polymer samples in TEM is challenging because of the thin sample requirement and because the high intensity of the electron beam can burn away polymer films before images can be produced.[46]

Scanning Electron Microscopy

Scanning electron microscopy (SEM) was used to determine particle size and distribution and to examine fracture surfaces. The SEM consists of an electron gun producing a source of electrons at an energy range of 1-40keV. Electron lenses reduce the diameter of the electron beam and place a small focused beam on the specimen. The electron beam interacts with the near-surface region of the specimen to a depth of about 1μm and generates signals used to form an image. The smaller the beam size, the better the resolution of the image. The SEM used for this study is capable of differentiating particle detail as small as 1 nm depending on elemental contrast and other parameters. The smaller the beam size, however, the less current available to form a clear picture. Operating the SEM requires fine tuning to optimize picture quality with resolution. SEM is run under a vacuum to minimize beam interactions with gas molecules which would retard resolution. Non-conductive specimens, such as most polymers, often suffer from variations in surface potential which introduce astigmatism, instabilities, and false x-ray signals. Charging, a condition during which charge accumulates on the surface of a non-conducting specimen causing excessive brightness, often occurs making it difficult to

obtain quality images. Sputter coating non-conductive samples with a fine gold layer is often required to avoid these issues.[47]

Fourier Transform Infrared Spectroscopy

Fourier transform infrared spectroscopy (FT-IR) was used to analyze the bonding between the polymer matrix and nanoparticles. FT-IR measures the absorption of infrared radiation by the sample material with respect to the wavelength of the radiation. Using absorption data, one may identify molecular components and structures. The signal detected is analyzed using Fourier transforms to provide infrared absorption spectra, usually presented as plots of intensity versus wavenumber (in cm^{-1}). Infrared wavelengths absorbed by a material identify its molecular structure. The absorption spectrum is most often compared against a spectrum from a known material for identification. Absorption bands in the range of 4000-1500 wavenumbers are typically due to functional groups such as –OH, C==O, N—H, and CH_3. The range from 1500-400 is referred to as the fingerprint region and generally caused by intra-molecular phenomena very specific to each material.[45, 48]

CHAPTER III

EXPERIMENTAL PROCEDURES

Initial System Mixture

Four polymer nanocomposite systems and two pure reference polymer systems were created following the same procedures. Sufficient quantity of solution of each system was made initially to support creation of samples for all mechanical characterization and analytical procedures. System portions for the four polymer nanocomposite systems were calculated to achieve 5% filler volume fraction in a 15% polymer weight fraction (to solvent) solution. System portions for the two reference polymer systems were calculated to achieve a 30% polymer weight fraction solution. The nanocomposite systems were prepared as lower weight fraction solutions to provide a less viscous environment into which the nanoparticles could be dispersed.

Table 1 provides the amounts of each component used to create the initial mixtures. All samples were mixed and stored in 500 ml Erlenmeyer flasks. Prior to use all lab equipment, including flasks, stirrers, spatulas, slides, etc., were first prepared by washing with Alconox soap and water, rinsing with acetone, rinsing with appropriate solvent, and then placed in a Fisher Scientific Isotemp dry oven for up to 30 minutes at 100˚C until dry.

Table 1. Portions used to make polymer and polymer nanocomposite systems.

System	Polymer (ml)	Filler (g)	Solvent (ml)
PS (pure/reference)	36.33	–	140
PS-Fe_3O_4	45.67	0.49	351
PS-Al_2O_3	36.54	0.50	281
PMMA (pure/reference)	32.48	–	110
PMMA-Fe_3O_4	36.54	0.44	220
PMMA-Al_2O_3	32.48	0.50	220

Alumina (Al_2O_3) nanoparticles, approximately 39 nm average diameter, were obtained from Nanophase Technologies. Magnetite (Fe_3O_4) nanoparticles, approximately 90 nm in diameter, were obtained from the University of Illinois. PS pellets, with 350,000 g/mol weight averaged molecular weight ($\overline{M}_W$), 1.040 g/cc density were obtained from Aldrich Chemical Company, Inc. PMMA granules, $\overline{M}_W$ = 350,000 g/mol, 1.170 g/cc density, were obtained from Aldrich Chemical Company, Inc. Density of alumina and magnetite was 4.00 g/cc and 5.15 g/cc respectively. Toluene (density 0.867 g/cc) obtained from Fisher Scientific was used as solvent for all PS-based systems. Chlorobenzene 99+% (density 1.106 g/cc) obtained from Acros was used as the solvent for all PMMA-based systems.

The same procedures were used to prepare samples for all systems. PS-Fe_3O_4 samples were created with the following method. A 500 ml flask, volumetric cylinder, spatula, and stirrer were prepared as described above. A 351 ml aliquot of toluene was measured and poured into the flask. The flask was placed on a Thermolyne Mirak stirring hotplate with the temperature set to 50˚C and revolutions set to 200RPM. A magnetic stirrer was dropped into the flask and began spinning. PS in the amount of

45.67 grams was measured and poured into the flask containing the toluene. Initially, the PS formed a viscous layer at the bottom of the flask. Flask temperature was raised to 70˚C. After several hours the mixture was clear and the stirrer was spinning freely, indicating that the polymer has dissolved. The stirrer was removed from the flask. Magnetite in the amount of 0.49 grams was measured and held in weighing paper. Flask was agitated on a Scientific Industries Vortex-2 Genie vortex with a setting of 8 to 10. While the mixture was swirling continuously the magnetite was slowly poured into the flask. Stirring continued for about 5 minutes. The flask was covered with American National Can Parafilm "M" laboratory film and stored in a fume hood.

The other systems were prepared in the same approach described above with some variations in temperatures used and time required to dissolve. Samples for all testing were created from the solutions produced from the procedures described above.

Tensile Testing

Tensile testing was used to provide elastic modulus and other mechanical properties. Creating tensile testing samples required significant time and effort. Samples for all six systems were created using similar procedures, although variations were used in attempts to improve the process and quality of samples. Tensile testing requires hardened 'dogbone' shaped samples created from the mixture described above. The biggest challenge in creating the sample was removing all the solvent and ensuring no air pockets existed in the neck region of the sample. Multiple samples were created for each system.

Following the guidelines provided in ASTM document D638, three aluminum molds were designed and manufactured in the Georgia Institute of Technology Mechanical Engineering machine shop. Two molds had approximate dimensions of 139 mm X 44 mm X 23 mm and consisted of removable top, bottom, and middle pieces, and another mold had slightly different dimensions as it was provided by another research group. Notches were cut into each side of the top and bottom pieces to ease removal of a hardened sample. Prior to use, all areas of the mold that would come in contact with the sample were sprayed with a mold release agent, Sprayon Dry Film P.T.F.E obtained from Lab Safety Supply. The mold release agent eased removal of the hardened samples.

After the mold was sprayed with mold release and allowed to dry, the top was removed from the mold and the mold was set on a level surface. The sample was poured into the mold until the solution reached the top edge of the mold. The mold was left in the hood for 24-72 hours while solvent evaporated. Air pockets existed in all samples after the solvent evaporated as shown in Figure 10(a). After the specified time of evaporation, a thin layer of sample covered the mold to a depth of 1 mm on the bottom and less thick on the sides. The sample was not completely hard, indicating that it still contained some amount of solvent. The mixture was poured again to the top edge of the mold. This process was repeated for total of 3-5 times, or until the mold was filled. After the last round of pouring, and sometimes after intermediate rounds of pouring, the mold was placed in a Fisher Scientific Isotemp dry oven at a temperature of 90-120˚C to speed solvent evaporation. Although this process removed the solvent more quickly it typically resulted in significantly more and larger air pockets, as shown in Figure 10(b).

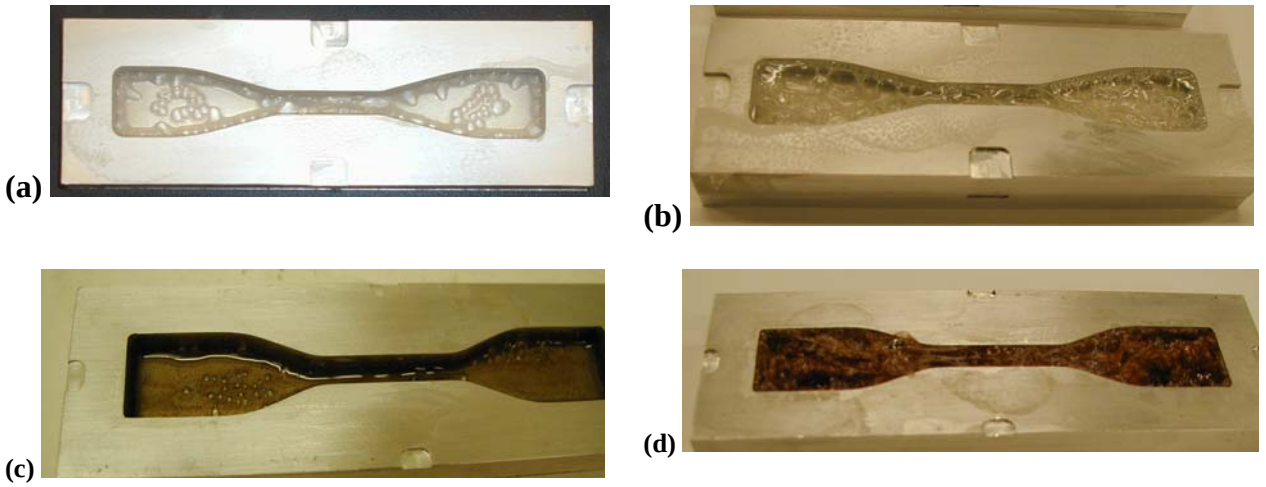

Figure 10. Dogbone samples at different steps during sample preparation process. (a) PS-Al_2O_3 system after first pouring of mixture and 24 hours in hood; (b) PS-Al_2O_3 system after second pouring of mixture and 24 hours in dry oven; (c) PS-Fe_3O_4 system after first pouring of mixture and 24 hours in hood; (d) PS-Fe_3O_4 system after fourth pouring of mixture and 48 hours in vacuum oven, just prior to compression molding.

Because of the significant volume of air pockets, the number of times the sample mixture was poured into the mold varied by system and solvent evaporation approach. After the solvent was evaporated in the dry oven on the last pouring of the mixture, the sample was placed in a Fisher Scientific Isotemp (Model 281A) vacuum oven to aid in removal of all remaining solvent. The sample was moved while still warm from the dry oven to the vacuum oven preheated to 90-140˚C. No ideal temperature was determined but most samples were heated to temperatures near 120˚C. If significant solvent was still present, movement of air bubbles could be observed. After no changes in the sample were observed for at least 1 hour, the vacuum was set to -28 in Hg (13.8 PSI, 711 torr). If a significant amount of solvent still remained in the sample, this increased vacuum caused significant increase in size of the air bubbles. In such cases, the vacuum was

intermittently purged and re-introduced until the sample stabilized. The mold was left in the vacuum oven at the chosen temperature and pressure for 24-72 hours. The dogbone sample at this point does not contain solvent but is filled with thousands of air bubbles ranging in size from 1 mm to 1+ cm.

In order to remove the air bubbles, each sample was compression molded in a Carver compression molding press. The top was placed on the mold, the mold was placed on the plates, and the compression molder was cranked closed until the top plate touched the mold. Moving the mold to the compression molder while it was still hot or after it had cooled did not seem to make a difference in the effectiveness of the process. The plates were heated to 130-190˚C. The mold was left in the compression molder prior to applying compression for at least 30 minutes to allow the temperature of the sample in the mold to equilibrate. The plates were cranked together periodically over a 1-3 hour period until a pressure of 2000PSI was reached, and the sample was left in the compression molder at this temperature and pressure for at least 1 hour. The press temperature was then set to room temperature and the sample remained under pressure for at least 6 hours or until it reached room temperature.

The sample was carefully removed from the mold and examined against a lighted backdrop to ensure no air bubbles existed. Many samples were discarded due to air bubbles remaining after compression molding. Figure 11(a) shows a good quality sample after compression molding versus a sample that must be discarded because of extensive air bubbles as shown in Figure 11(b). The edges of the sample were smoothed with a razor blade and sandpaper. The width and thickness of the sample's neck were measured in three places with an outside micrometer from Mitutoyo Corporation to an accuracy of

1 micron. The magnetite samples were dark brown in color and opaque as shown in Figure 11. The alumina based samples were light yellow in color and slightly translucent, as shown in Figure 12. The thickness of the finished dogbone samples ranged from 1-2.5 mm.

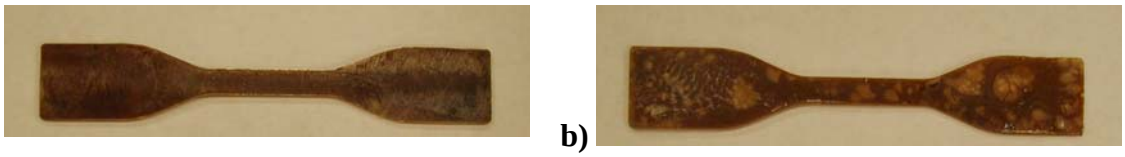

Figure 11. Dogbone samples after compression molding: a) good quality dogbone sample for the PMMA-Fe_3O_4 system; b) unusable dogbone sample for the PMMA-Fe_3O_4 system because of air bubbles throughout neck.

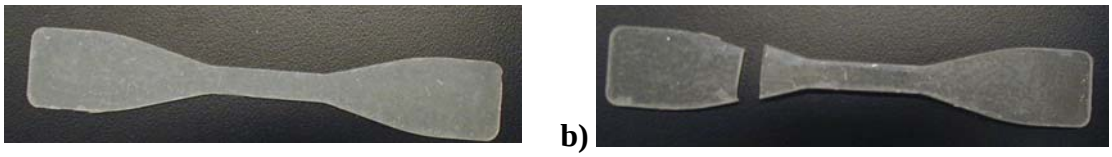

Figure 12. Dogbone samples after compression molding: a) good quality dogbone sample for the PMMA-Al_2O_3 system; b) unusable dogbone sample for the PMMA-Al_2O_3 system because it broke while being removed from the mold.

Tensile testing was performed using MTI Phoenix tensile testing equipment with a 10 Kip (10,000 pound-force, 44.48 kilonewton) and a ±0.2 inch Instron extensometer. The load cell and extensometer were calibrated prior to use. Double sided tape was wrapped around the sample where the extensometer attached and three 6 mm GAC H6 Elastics Heavy rubber bands were used to secure each end of the extensometer to prevent slipping. Output from the extensometer was confirmed to be 0.0V or +0.2V prior to applying load. Load was applied at a displacement rate of 0.1 in/min. Initial load was set

to 0.5 pounds. A separate text output file for each sample included time, load, and displacement in volts. Two to five tensile tests were performed for each system.

In order to analyze the data, all tensile testing output files were read into Microsoft Excel. Load was converted to stress, σ, using $\sigma = \frac{F}{A}$, where F is the force applied as reported from the tensile testing equipment, and A is the cross sectional area calculated from the average of the sample's neck measurements. Displacement was converted to millimeters and strain, ε, was calculated using $\varepsilon = \frac{\Delta l}{l_o}$, where Δl is the change in length of the sample as converted from extensometer voltage output data, and l_o is the original extensometer gage length, or 25.4 millimeters.

A stress vs. strain curve was plotted from the data and modulus, E, was calculated as the slope of the initial linear portion of the curve, or $E = \frac{\Delta \sigma}{\Delta \varepsilon}$. The first point used in calculating the modulus was taken at approximately 5 MPa of stress, above the load take-up region, and the last point was taken at the highest stress before the curve became non-linear. The values were visually determined from the stress versus strain plot but pulled directly from the Excel data for calculations. Ultimate stress and strain were taken as the maximum values at the sample fracture point, as determined in the plot and the data. Results from multiple tests were averaged for each system.

Nanoindentation

Nanoindentation was used to determine elastic modulus and hardness properties. Samples for nanoindentation must be flat and can be as small as microns thin and millimeters wide or long. Thin film samples on glass slides were created to support nanoindentation. Samples for all six systems were created using similar procedures, although slight variations were used in an attempt to minimize air bubbles in the samples.

Procedures to make samples for the PS-Fe_3O_4 system will be provided, with all other systems following similar steps. A glass slide was cleaned as described above, labeled, and placed on a level surface. The PS-Fe_3O_4 mixture was poured on the slide until it filled a majority of the slide's surface. The slide was placed in the hood for 24-72 hours while solvent evaporated. The slide was placed in a Fisher Scientific Isotemp vacuum oven at 90-140˚C with no vacuum to help with solvent evaporation for at least 2 hours. Depending on the system, air bubbles typically appeared at this point in the process with PS-based systems showing significantly more bubbles. After no rising or emergence of bubbles was observed in the sample for at least 1 hour, the vacuum was set to -28 in Hg (13.8 PSI, 711 torr). After 2-12 hours, the vacuum was removed and the temperature was decreased to room temperature. The sample was allowed to cool in the oven. For samples with significant air bubbles, a flat portion of the thin film was cut out and the rest of the sample was discarded. The slide was affixed using "Super Glue" brand cyanoacrylate adhesive to a sample plug created in a Simplimet 2000 Automatic Mounting Press. Typical thickness of samples on the slides was 200-1000 microns.

Nanoidentation was performed on a MTS Nanoindenter using the DCM indenter head and a Berkovich shaped diamond indenter operated in batch mode by MTS TestWorks4 controller software. Multiple batch runs with 4-9 offset tests per batch were run for each sample, and the distance between each test indentation location was set to 20-30μm in the X and Y directions. Parameters set for test runs included: Allowable Drift Rate to 0.150 nm/s, Depth Limit to 200-500 nm, Frequency Target to 0.45 Hz. Poisson's ratio was set to 0.375 for PMMA- and 0.350 for PS-based systems.[49] Starting indention locations on the sample for batch runs were chosen randomly but were visually checked via the video viewer to ensure the test did not take place near an air bubble. Most batches were scheduled to run overnight to ensure the quietest environment. Batch test results were discarded if any tests within the batch failed. The MTS TestWorks4 software calculated hardness and elastic modulus automatically so results were simply summarized and reported.

DMA

DMA was used to determine elastic modulus properties of all six systems. DMA accepts several different forms of samples. Equipment available for this study required small rectangular samples approximately 25 mm long, 5-10 mm wide, and 0.100-2 mm thick. To meet this requirement, thin film samples on glass slides were created. Samples were prepared by the approach described above in nanoindentation experimental procedures. For this technique, however, enough mixture was poured to cover the entire slide. Because the slides were approximately 25 mm wide this approach allowed cutting

multiple samples from the same slide. However, since many of the samples, and especially the PS-based samples, contained air bubbles, often only a few usable samples were taken from each thin film. Samples were cut from the slides using a low speed diamond wheel saw. Each sample was labeled with a marker, and width and depth were measured and recorded at two places on each sample.

Figure 13. DMA samples for PS-Fe_3O_4 system.

DMA tests were performed on a Rheometric Scientific III Dynamic Mechanical Analyzer using RSA Orchestrator v6.58B2 software. Parameters set for tests included: 10 mm gap distance, Rectangular Tension/Compression geometry, strain-controlled test type. Sample geometry was input for each sample. At least one tensile test for each system was performed on the DMA equipment to determine the static initial load. For tensile testing the test mode was set to "Multiple Extension Mode Test", measurement type was set to "transient", and data points per zone was set to 350. Although the DMA was configured with two transducers, the maximum transducer load was 3500 grams so tensile testing had to be manually stopped prior to sample breakage so that the transducer did not overload. Once the tensile test completed, the stress vs. strain report produced by

the software was observed and an initial static force used for dynamic testing was chosen. Given the stress limits, tensile testing only served to indicate the proper initial static load.

Dynamic testing was performed on two to seven samples for each system. Parameters were the same as for tensile testing except test mode was "Dynamic Temperature Ramp Test", measurement type was "dynamic", 1.0Hz frequency, 30˚C initial temperature, 150˚ final temperature, 2.0˚C/minute ramp rate, 0.1% strain rate, and initial static load of 100-250 grams. Initial static load was chosen to be 0.5% to 1% strain in the tensile testing results. Parameters were chosen based on review of literature and discussions with experienced DMA researchers.

In DMA, the glass transition temperature, T_g, of a sample can be accurately determined from the elastic and loss modulus response to temperature and stress. Most tests, however, were manually stopped prior to reaching T_g because the sample either collapsed or broke. Even though the data near the higher temperature end of each test was considered invalid, the initial elastic modulus near room temperature was considered accurate.

Results were analyzed by averaging the elastic modulus data point at a specific temperature for multiple runs of a particular system.

TGA

TGA was used to determine the impact of the presence of nanoparticles on decomposition temperature and to estimate the thickness of the polymer layer adsorbed to the nanoparticles. Two types of samples were prepared for TGA. Thin film samples on

slides were prepared to determine decomposition temperatures and samples of polymer-capped nanoparticles were prepared for determining the polymer layer thickness.

TGA thin film samples were prepared for each of the six systems by the approach described previously in nanoindentation experimental procedures. A razor blade was used to cut small pieces of the sample to fit in the TGA pan.

TGA capped nanoparticle samples were prepared by two different methods. Both methods involved pouring a 30-40 ml aliquot of the initial system mixture into a prepared vial. The goal of both methods was to separate the excess polymer and solvent from the polymer-coated nanoparticles. The first method relied on precipitation of particles from the solution over time. The closed vial containing the mixture was left undisturbed for 24-36 hours while a layer of precipitated capped particles formed at the bottom of the vial. The liquid portion of the vial was poured out and discarded, being careful not to lose any particles. The vial was refilled with solvent and the vial was shaken using a Scientific Industries Vortex-2 Genie vortex for 1 minute to remove any excess unbound polymer from the particles. The closed vial was left undisturbed for another 24-36 hours while the layer of precipitated capped nanoparticles formed at the bottom of the vial. Figure 14 shows a vial in the process of precipitating the nanoparticles. This process was repeated 4-5 times so that the final solution contained only solvent and fine particles with no visible excess polymer.

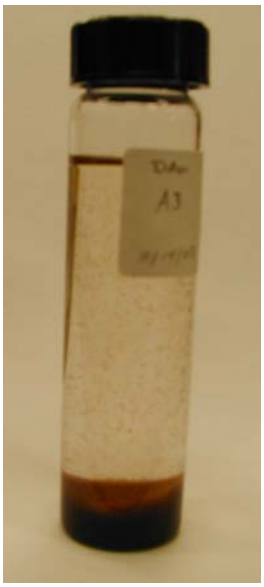

Figure 14. Vial of PMMA-Al_2O_3 capped particles. Nanoparticles can be seen suspended in the solvent and there is precipitate at the bottom of the vial.

The second method of preparing capped particle samples used a centrifuge to speed the precipitation of the particles. The particles in the vial were centrifuged using a Fisher Scientific Centrific Model 228 centrifuge at 10,000 – 15,000 RPM for 12-17 minutes. The capped particles formed a solid mass at the bottom of the vial. The excess polymer and solvent solution was removed and the remaining particles were washed with solvent to remove any excess unbound polymer. The vial was shaken using a Scientific Industries Vortex-2 Genie vortex for 1 minute to remove any excess unbound polymer from the particles. The suspension was centrifuged again. This process was repeated 3-4 times. As will be discussed in the results section, both approaches provided similar TGA results.

TGA experiments were performed using a TA Instruments TGA Model 50 with a platinum sample pan. Thin film sample sizes were 8-12 mg, while capped particle

samples were 2-4 mg. Prior to performing any TGA experiments, the equipment was weight calibrated according to instructions provided by the manufacturer. For each experiment, the pan was cleaned with soap and water and any visible residue was removed. The empty pan was then run through a 'burn-in' process in which a TGA "ramp" procedure of 100˚C/min to 800˚C was performed to ensure that the pan environment was clean for the experiment. The pan was then tared to establish its empty weight. Once the system temperature returned to room temperature, the sample was placed in the pan and weighed by loading the sample into the TGA, and ensuring the weight was within the expected range. TGA was then performed at a ramp rate of 10˚C/min to 600˚C. Nitrogen balance and sample flow rates were 40.0 and 60.0 ml/min, respectively. Individual sequence files detailing the experimental parameters were saved for each experiment.

Using TA Instruments Universal Analyzer software data was exported into Microsoft Excel. The software outputs time, temperature, and weight for over 3500 data points through the temperature range. To reproduce the plot available in the software with the data in Excel, weight fraction remaining (weight %) was calculated from the initial weight and plotted against temperature.

TEM

TEM was used to characterize the size of the particles present in the four nanocomposite systems. The initial goal for using TEM was to provide a clear indication of size and distribution of the nanoparticles embedded in the polymer matrix. The

necessity for thin samples presents a challenge for polymer samples. TEM must be placed on a wire mesh grid and ideally the sample is less than 100 nm thick. One way to create a thin TEM sample with polymer solutions is to dilute the solution and dip the grid in the diluted solution to form a film on the grid and assume that nanoparticles are transferred to the grid with the polymer solution. Diluting the polymer nanocomposite solution by the appropriate amount is a trial and error exercise. For the four polymer nanocomposite systems, several small vials were partially filled with the initial system solution and incremental amounts of solvent were added to create a range of dilutions. A Formvar coated 200 mesh carbon film copper grid from Ted Pella, Inc. was dipped into the diluted solution, then its edge was touched to a Kimwipe to drain away the excess solvent. For each system, sample grids were made for each dilution using this process. Sample grids were examined using a JEOL 100C TEM at 100kV power. The correct dilution, unfortunately, was never reached. Some samples were too thick and appeared dark under TEM. In the more dilute solutions no nanoparticles adhered to the grid and the sample appeared to be an empty grid.

As an alternative approach, capped particles were suspended in solvent and a grid was dipped into the solution as described above. Although several times no particles adhered to the grid, some samples were successfully made using this approach. Because capped particles were already removed from the polymer matrix, these images did not provide any particle distribution information. In fact, given the tendency of nanoparticles to flocculate, many grids contained huge flocculates of capped particles. However, many smaller particles were also visible throughout the grid. Using these samples TEM provided insight into only the possible size of the particles in the matrix.

SEM

SEM was used to determine size and distribution of particles in the dogbone samples for the four polymer nanocomposite systems. After tensile testing, approximately a 5 mm section of the sample neck, including one fracture surface, was cut and placed on a SEM sample holder. Carbon tape was place under the polymer sample and a small roll of carbon tape was placed against the sample to stabilize it on the sample holder. Because polymers are generally non-conductive and would experience charging in the SEM, the samples were sputter coated with gold using an International Scientific Instruments sputter coater. Covering the samples with a thin layer of gold atoms reduces or eliminates charging issues. After evacuating the sputter coater chamber to 0.7 torr, the samples were sputtered coated for only 80 seconds to minimize the thickness of the gold layer to minimize distortion of the surface detail.

SEM was performed in a LEO 1530 Thermally-Assisted FEG Scanning Electron Microscope at 10kV. Several pictures were taken of each sample. Images were opened with Adobe Photoshop 5.5 and each particle was measured using the software's "Measure Tool". The micron bar on the image was also measured and its length was compared against the actual size labeled on the bar. The size of the particle was calculated based on the ratio of the particle to micron bar and the stated size of the micron bar, as shown in equation (1).

$$particle\ size = \text{particle measured dimensions} \times \frac{\text{bar\_labeled\_size}}{\text{bar\_measured\_dimensions}} \qquad (1)$$

Particle sizes were averaged for a polymer nanocomposite system to achieve a standard particle size with a standard deviation.

FT-IR

FT-IR was used to identify the bonding between the polymer matrix and nanoparticles. Analyzing spectra requires detailed knowledge of which peaks indicate which bonds. Because PMMA data was readily available and the bonds between the PMMA matrix and nanoparticles were expected to be more pronounced, FT-IR of only the two PMMA-based samples was performed. Prior to executing any tests the Spectra-Tech liquid demountable cell with a 0.2 mm Teflon spacer and KBr windows was dismantled, cleaned with Kimwipes and solvent, and reassembled. The cell was placed into a Nicolet Instrument Corporation Nexus 870 FT-IR spectrometer, and after the infrared sample compartment was sealed and purged for at least 5 minutes, a background spectra was taken and assigned for use on subsequent spectra acquisitions. The vials containing the centrifuged capped particles were shaken using a Scientific Industries Vortex-2 Genie vortex to re-suspend the particles. A disposable pipette was used to transfer an aliquot of the capped particle suspension to the cell, ensuring that no air bubbles remained in the cell. The cell was placed into the spectrometer and the sample compartment was sealed and purged for at least 5 minutes. The sample spectrum was acquired and stored for further analysis. Using Nicolet OMNIC 5.2a software the spectrum was compared against a previously recorded spectrum of PMMA and

chlorobenzene solvent. By comparing specific capped particles peaks to PMMA/chlorobenzene peaks, bonding unique to the capped particles was highlighted. Using peak height analysis tools within the software, specific peak wavenumber and baselined peak heights were recorded.

CHAPTER IV

RESULTS AND DISCUSSION

In order to characterize the impact of nanoparticles on the mechanical properties of polymer composites, this study used three different mechanical testing techniques: tensile testing, DMA, and nanoindentation. Each technique determines the elastic modulus for the specimen, as well as other properties specific to each technique. First, the results of the three techniques will be summarized and the results will compared. Second, specific results from each of the individual techniques, as well as particle size and particle dispersion results, will be presented. Third, the interphase will be characterized employing two different characterization techniques, and their results will be evaluated to explain the mechanical testing results.

Mechanical Characterization

Mechanical Testing Results Summary

This study included performing the three mechanical testing techniques on the two polymer reference systems and on the four polymer nanocomposite systems. All samples were prepared using the same procedures and all mechanical tests were run using the same parameters. This consistent approach to testing provided a true comparison between the reference pure polymer systems, PMMA and PS, and the nanocomposite

systems, PMMA-Al_2O_3, PMMA-Fe_3O_4, PS-Al_2O_3, and PS-Fe_3O_4. The combined elastic modulus results of all three testing techniques are shown in Figure 15.

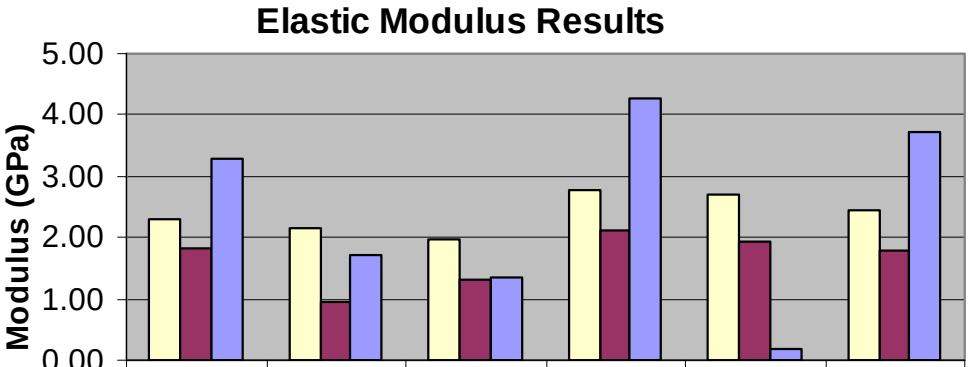

	PMMA	PMMA-Al2O3	PMMA-Fe3O4	PS	PS-Al2O3	PS-Fe3O4
Tensile	2.29	2.15	1.97	2.76	2.68	2.46
DMA	1.84	0.95	1.32	2.12	1.95	1.78
Nanoindenter	3.27	1.73	1.36	4.25	0.17	3.74

Figure 15. Elastic modulus results for tensile testing, DMA, and nanoindentation mechanical testing.

The results of all three techniques showed a decrease in modulus of the nanocomposite systems as compared to the pure systems. These results contradict the theory that nanoparticle fillers improve the composite's mechanical properties, specifically the elastic modulus. Examining the percent change of modulus of the nanocomposites over the pure systems allows for more quantitative analysis of the results. Table 2 summarizes the change in modulus with the addition of nanoparticles.

Table 2. Summary of impact on modulus from addition of nanoparticle fillers to PMMA and PS matrices from tensile testing, DMA, and nanoindentation mechanical testing.

Sample	% Chg Tensile Testing	% Chg DMA	% Chg Nanoindentation
PMMA			
PMMA-Al_2O_3	-6%	-28%	-47%
PMMA-Fe_3O_4	-14%	-49%	-59%
PS			
PS-Al_2O_3	-3%	-16%	-96%
PS-Fe_3O_4	-11%	-8%	-12%

Table 2 shows some interesting trends. In all but one case, nanoindentation provided the higher modulus values for a particular system, with DMA providing the next highest, and tensile testing providing the lowest modulus values. Among the three testing techniques, nanoindentation is most affected by local properties. Viscoelastic behavior affects the shape of the unloading curve, resulting in modulus values higher than bulk values.[50] Several other studies have concluded that the modulus determined at or near the surface can be quite different from that of the bulk material.[41] The higher nanoindentation values found are not surprising since other research has shown these similar trends.[50] Lucas, et al. reported modulus for nanoindentation as 1.2GPa, 0.5 for DMA, and 0.4 GPA for tensile testing of poly(tetrafluoroethylene).[50] More directly related to this current work's results, Kourtesis, et al. determined the modulus of PMMA to be 3.27 GPa with nanoindentation and 1.55 GPa with tensile testing.[50] The nanoindentation modulus matched exactly the 3.27 GPa value found in this study, as shown in Figure 15.

Although the different techniques yielded different modulus ranges, the trend in each test was consistent; nanoparticle fillers do not increase the modulus in these

systems. In order to explain the differences in the modulus ranges across techniques, one can consider the nature of the sample and the testing approach. With these considerations, one would describe tensile testing as examining properties of the bulk material, DMA examining properties of more localized but still bulk material, and nanoindentation examining properties locally.

The role of interphase in the mechanical results is examined in detail in a subsequent section, but one can predict the structure based on the modulus results. In the PMMA-based systems, the Fe_3O_4 filler provided a consistently lower modulus than that provided by the Al_2O_3 filler in all three testing techniques. The higher reactivity of Al_2O_3 [5] over Fe_3O_4 serves to form a denser interphase with the matrix, resulting in an modulus higher than the less dense Fe_3O_4 interphase. For PS-based systems, all but tensile testing showed Al_2O_3 with a modulus higher than Fe_3O_4. Additional results and observations are provided for each technique in the following sections.

Tensile Testing

Tensile testing was performed to determine the bulk mechanical properties of polymer nanocomposites. Because factors such as molecular weight, tacticity, and processing history impact polymer mechanical properties, pure polymer reference systems were tested to ensure a more direct comparison with nanocomposites. Using pure polymer references for comparison that undergo the same processing as the nanocomposites enhances the reliability of the data. Tensile testing data was plotted in stress versus strain curves, examples of which are shown in Figure 16. Elastic modulus is defined as the slope of the linear portion of the stress/strain curve. Choosing the

appropriate data limits to use in calculating the modulus requires visually evaluating the curves. The linear portion of the curves for most systems was determined to be between 5 MPa and 15 MPa stress.

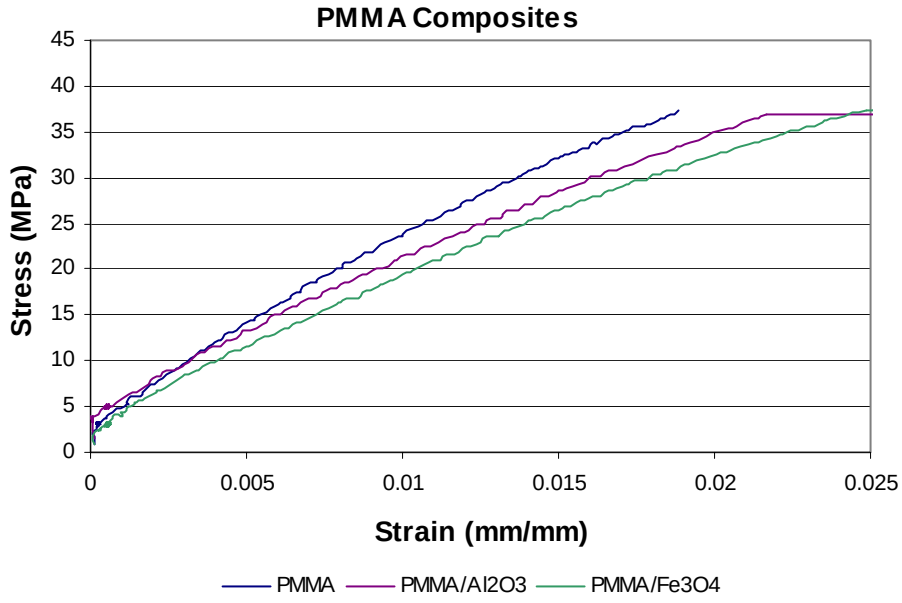

(a)

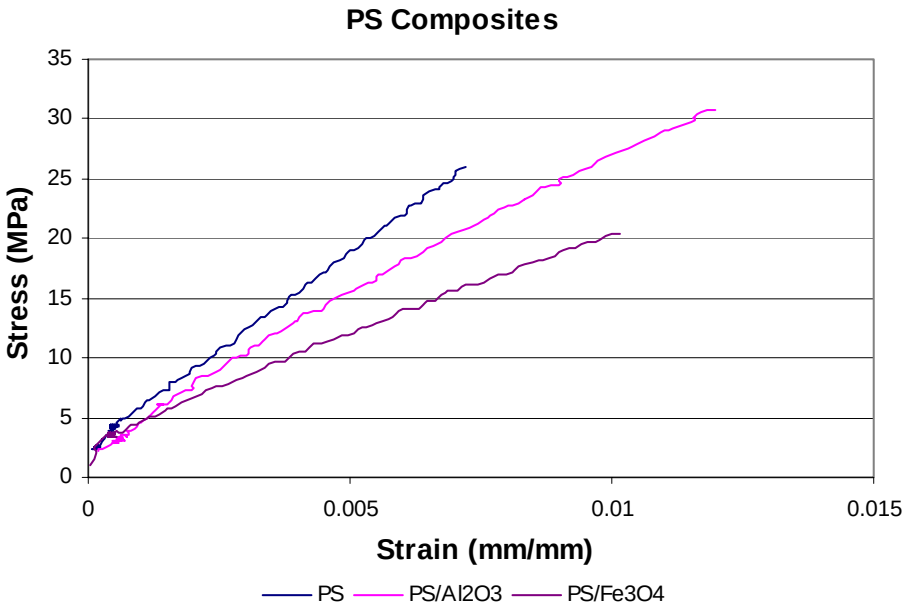

(b)

Figure 16. Tensile testing stress versus strain curves for (a) PMMA and PMMA nanocomposites, and (b) PS and PS nanocomposites.

Summarized tensile testing results, depicted in Figure 17, show that elastic modulus decreased slightly with the addition of either Al_2O_3 or Fe_3O_4 nanoparticles. The data for each system is compiled from an average of all test results for the system, and the error bar indicates the standard deviation of all tests for that system.

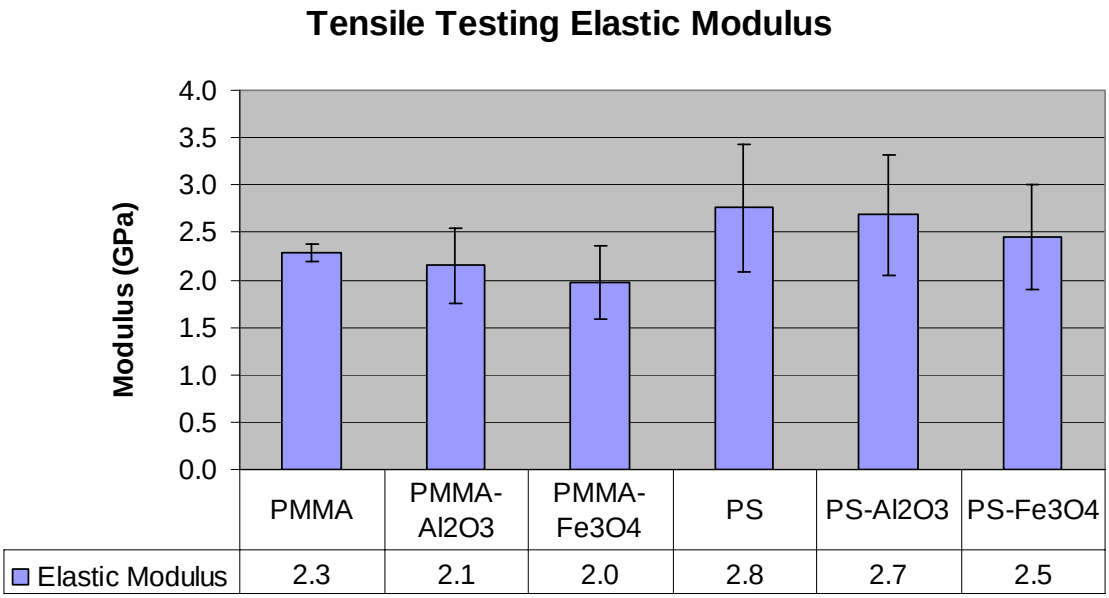

Figure 17. Tensile testing elastic modulus summary results.

The decreasing trend in modulus is consistent across the two polymer and associated nanocomposite systems, but the difference in each system is within the range of experimental error. These results seem to contradict the theory that nanoparticle fillers should improve the mechanical properties, specifically the elastic modulus, of polymer nanocomposites over pure systems or micro-sized fillers. In one of the few studies that have mechanically characterized similar systems, Ash, et al. showed a 15% decrease in elastic modulus for the PMMA-Al_2O_3 system.[17] Considering a reasonable margin of error, the 6% decrease found in this study, as shown in Table 2, conforms with those

results. Additionally, Ash, et al. found that PMMA-Al_2O_3 showed a 20% decrease in ultimate stress, but a 600% increase in ultimate strain.[17] Figure 18 provides the detailed results of ultimate stress and strain results from tensile testing and Table 3 summarizes the results.

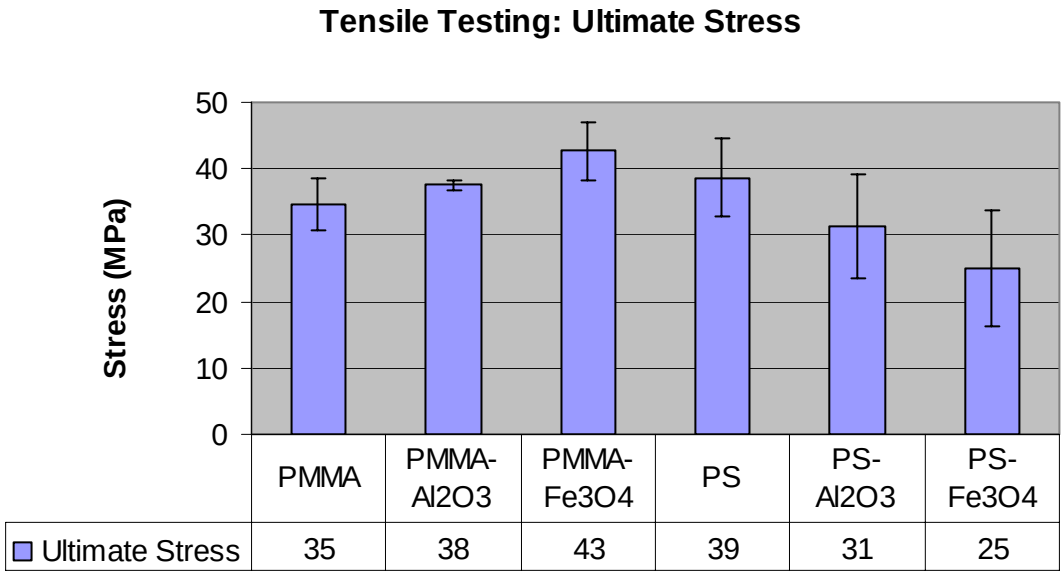

(a)

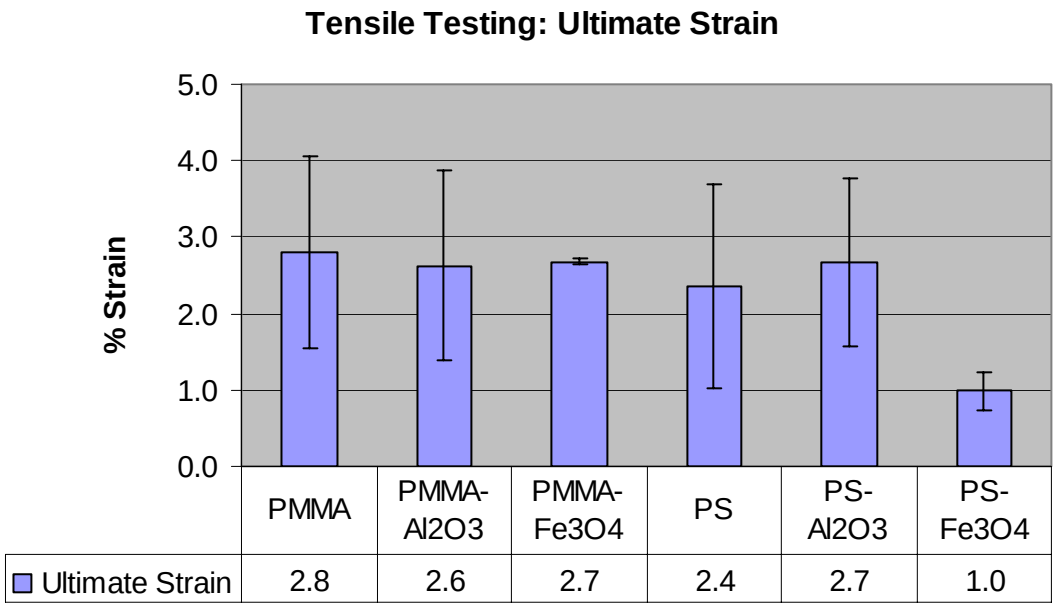

(b)

Figure 18. Tensile testing results: (a) ultimate stress, and (b) ultimate strain.

Table 3. Summary of tensile testing ultimate stress and ultimate strain results with respect to pure polymer samples.

Sample	Ultimate Stress	% Chg	Ultimate Strain	% Chg
PMMA	34.6		2.8	
PMMA-Al_2O_3	37.5	9%	2.6	-6%
PMMA-Fe_3O_4	42.6	23%	2.7	-4%
PS	38.7		2.4	
PS-Al_2O_3	31.3	-19%	2.7	13%
PS-Fe_3O_4	25.0	-35%	1.0	-58%

The current study yielded ultimate stress and strain results different than those found by Ash, et al. Tensile testing showed a slight increase of 9% in ultimate stress of PMMA-Al_2O_3 instead of the 20% increase provided by Ash, et al. The 6% decrease in ultimate strain found in this study is opposite of and an order of magnitude smaller than the results experienced by Ash, et al. Also, they saw a well defined yield point in the nanocomposite stress versus strain curve, which is not observed in this study's results. Differences between the results could stem from sample preparation and particle dispersion differences. Although Ash, et al. used the same alumina pre-made particles and created the dogbone samples using compression molding, they did not provide details of sample preparation such as whether the dogbone samples experienced bubbling during solvent evaporation or whether air bubbles existed in the samples. Ash did indicate that the particles were well dispersed and consistently 39 nm in size. As will be discussed later, the dispersion and particle size in this study are likely not as well dispersed.[17]

Table 3 shows that ultimate stress increased for both PMMA-based nanocomposites but decreased for both PS-based nanocomposites. Ultimate strain decreased slightly for both PMMA-based nanocomposites but was inconsistent for both

PS-based nanocomposites. Note that the large standard deviation of results in ultimate strain, as shown in Figure 18(b), casts doubt on any conclusion drawn on the data. As discussed in the Background section of this paper, few conclusive trends exist for the impact of nanocomposites on ultimate stress and ultimate strain.

DMA

DMA was performed to determine the bulk mechanical properties of polymer nanocomposites. Prior to executing dynamic tests, static tensile tests were run on the equipment to determine the optimal static initial load. Dynamic testing results were processed by the computer software and provided as a plot of storage (elastic) modulus, loss modulus, and tan δ versus temperature. Very few of the tests ran to completion, primarily because of sample buckling and equipment limitations. But, because the goal of using modulus results was for direct comparison between the nanocomposites and the pure polymer reference systems, the room temperature modulus was the primary result evaluated. Figure 19 shows sample output from a DMA test of the PS-Al_2O_3 system for a test that ran nearly to completion. The peak of the red tan δ curve provides the glass transition temperature of the nanocomposite. Because so few tests ran to the point of reaching a maximum in tan δ, the current study will not report glass transition temperatures from DMA.

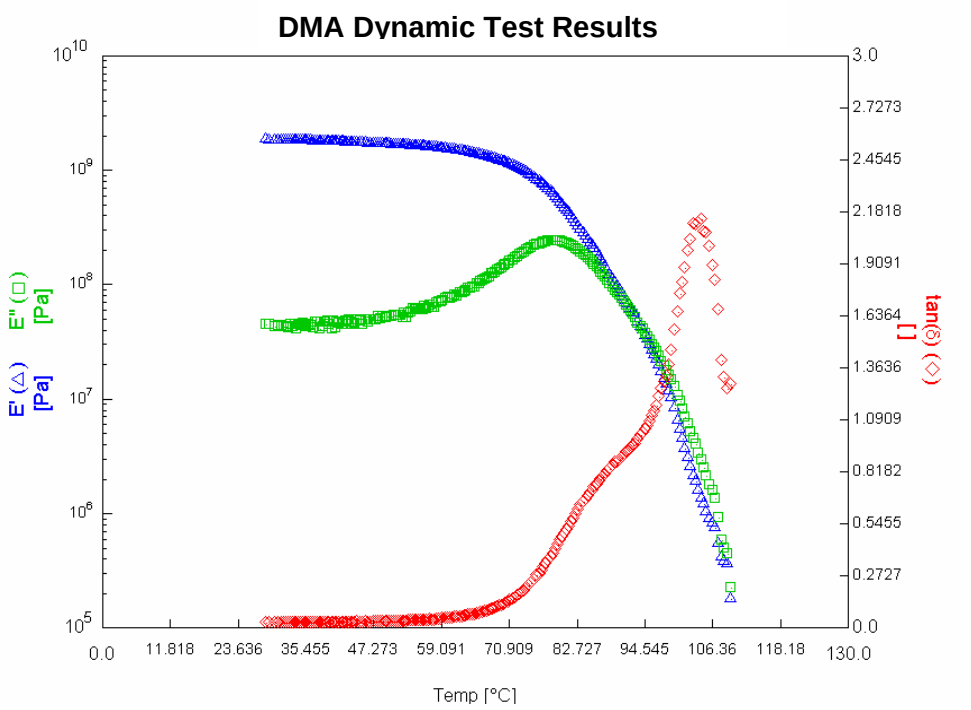

Figure 19. DMA dynamic test results for PS-Al_2O_3 nanocomposite system that ran nearly to completion, giving a maximum tan δ, or glass transition temperature.

Figure 20 shows a more typical result from DMA testing. The PS-Al_2O_3 sample buckled prior to reaching a maximum tan δ and the test had to be manually stopped.

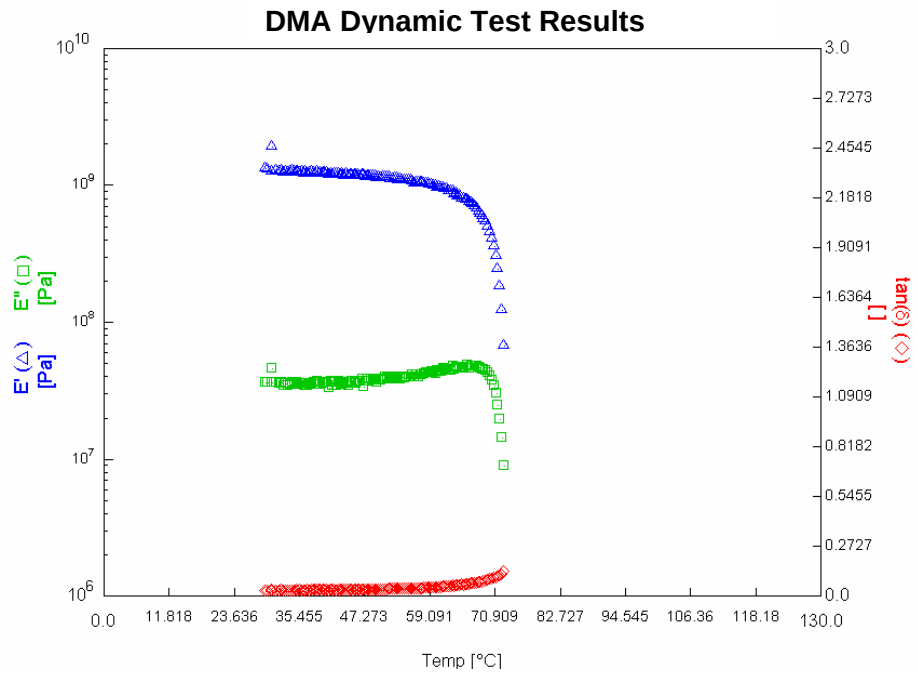

Figure 20. DMA dynamic test results for PS-Fe_3O_4 nanocomposite system in which sample buckled prior to reaching its glass transition temperature.

DMA results for the nanocomposite systems show a consistent trend of decreased elastic modulus over the pure polymer reference systems, as shown in Figure 21. The consistency of this trend with the tensile testing results strengthens confidence in these results. The standard deviation, shown as error bars in Figure 21, however, suggests the conclusions are less clear. The reason for variance in results across tests is likely caused by challenges with the testing procedures. Because DMA is performed on small samples, sliced from thin films, errors in geometrical measurements are more significant than errors would be in measuring larger samples. Additionally, the test equipment had faulty grips, and several tests were discarded because the sample slipped from the grips during testing. All results from tests in which the sample did not slip were retained and reported.

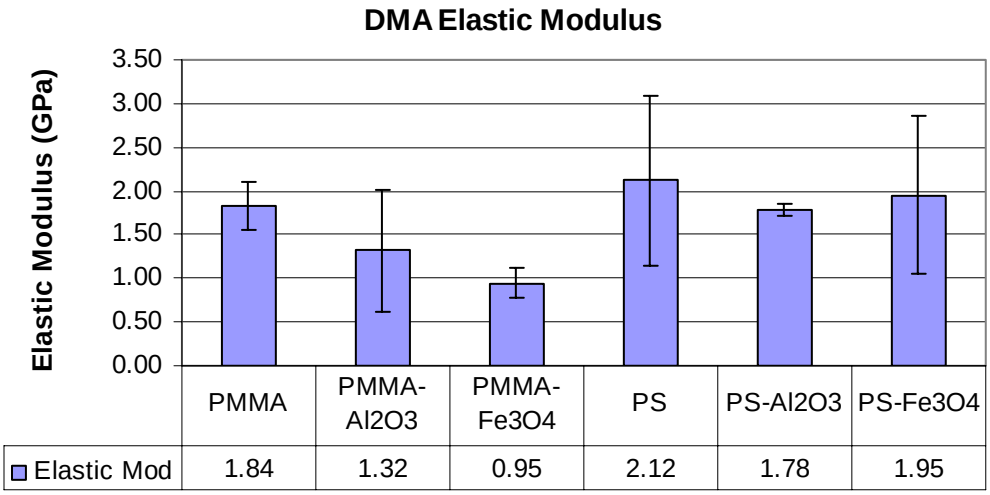

Figure 21. DMA elastic modulus summary results.

Loss modulus is the capacity of a material to dissipate energy when placed when stressed. Theoretically, the addition of filler to a polymer matrix should increase the loss modulus. As the polymer segments bond to the surface, the loops and chains that extend toward the bulk matrix are expected to support a mechanical interlocking with the bulk chains. This interaction can be effective in transmitting stress between the matrix and the filler.[20, 39] Loss modulus results from DMA, however, do not follow the expected trend. As shown in Figure 22, loss modulus of the PMMA-based nanocomposites is lower than that of the pure material. Although the PS-based systems results are extremely close, the loss modulus does decrease slightly with the addition of nanoparticles. Once again, the error bars in the chart provide standard deviation of the results.

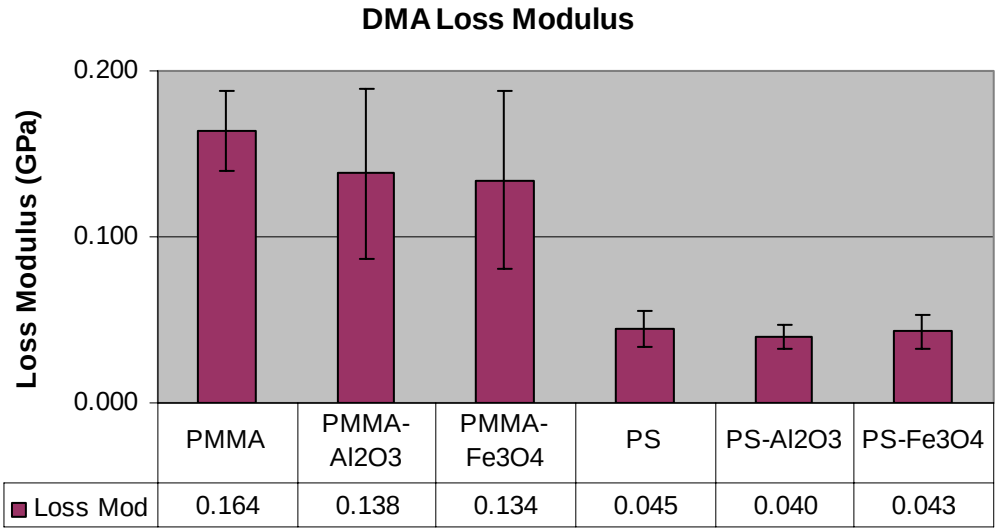

Figure 22. DMA loss modulus summary results.

Nanoindentation

Nanoindentation was performed to determine the localized mechanical properties of polymer nanocomposites. Thin film samples were prepared and tested for all systems. The parameters used for each test series were the same except for the different Poisson's ratios for PS and PMMA. Nanoindentation software performed all calculations of elastic modulus and hardness based on the input parameters, and generated a graph plotting modulus relative to indentation depth for each set of batch tests, as shown in Figure 23. Note that nanoindentation provides both load and unload elastic modulus and hardness data for each test, but the unload data is most representative of the material properties.

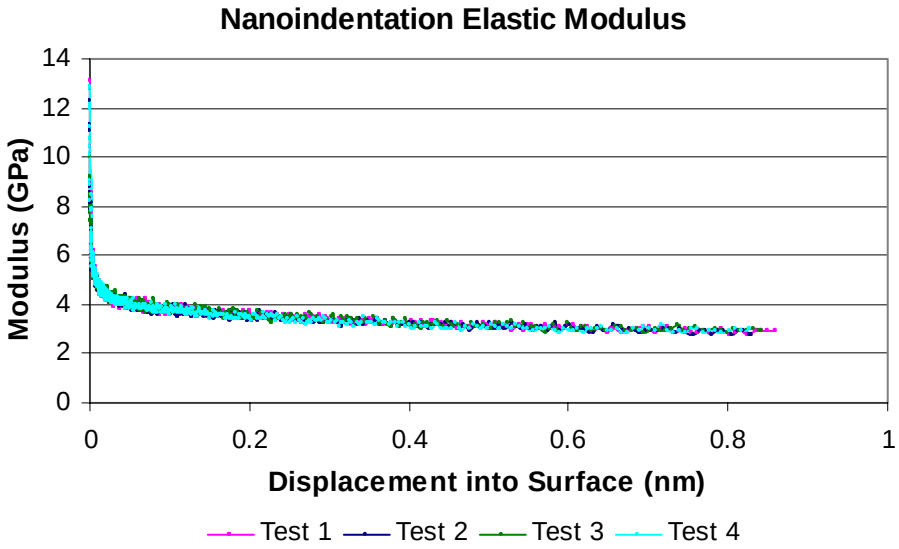

Figure 23. Nanoindentation elastic modulus results for a PMMA-Al_2O_3 batch test.

Nanoindentation elastic modulus trends were consistent with those of tensile testing and DMA results; these nanocomposite systems exhibit lower modulus relative to their pure polymer counterparts, as shown in Figure 24. As discussed earlier, nanoindentation calculations of modulus tend to be higher than those of the other methods, and the results generally confirmed the supposition, except in the case of the PMMA-Fe_3O_4 and PS-Al_2O_3 systems. The PS-Al_2O_3 system, however, had extremely low modulus, which would suggest sample issues or indentation location issues.

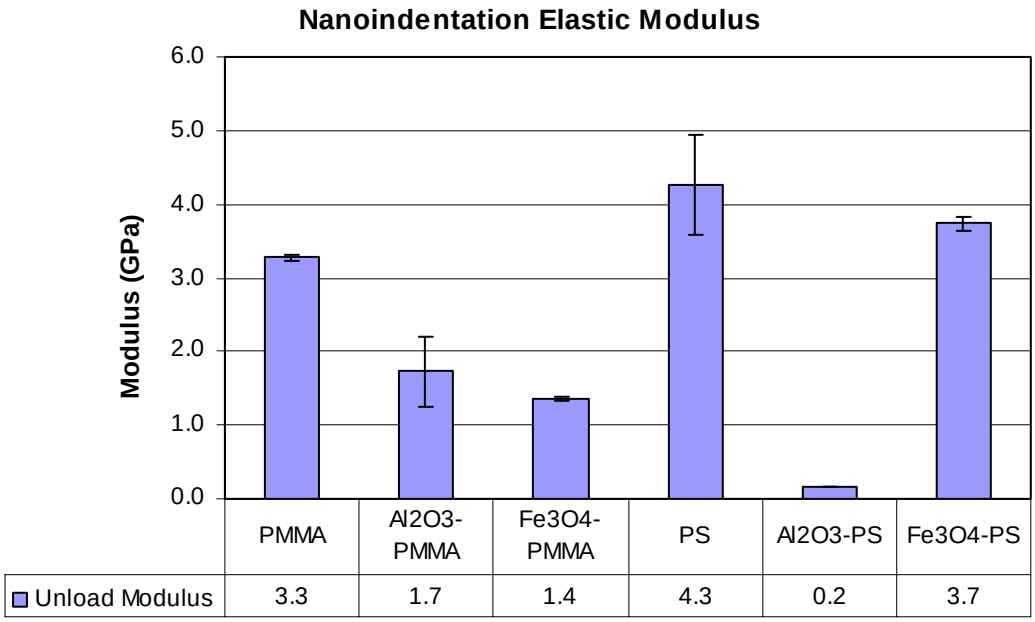

Figure 24. Nanoindentation unload elastic modulus summary results.

One potential concern regarding nanoindentation of polymer thin film samples is the impact of the substrate, that is, the glass slide on which the film lays, on the indentation results, which is a factor of the indentation depth and the sample thickness. Research recommends indentation depths no more than 10% of the sample thickness.[42, 51] The substrate is not a factor in the current study's results because the samples were at least 200 μm thick and the indentation depth was at most 500 nm, which is less than 1% of the sample thickness.

Nanoindentation also provides unload hardness results, as shown in Figure 25. The results follow the same trend as elastic modulus results; a decreased hardness for nanocomposites over their pure polymer counterparts. This consistency is not surprising, however, because other studies also have shown a linear relationship between nanoindenter hardness results and tensile testing strength results.[52]

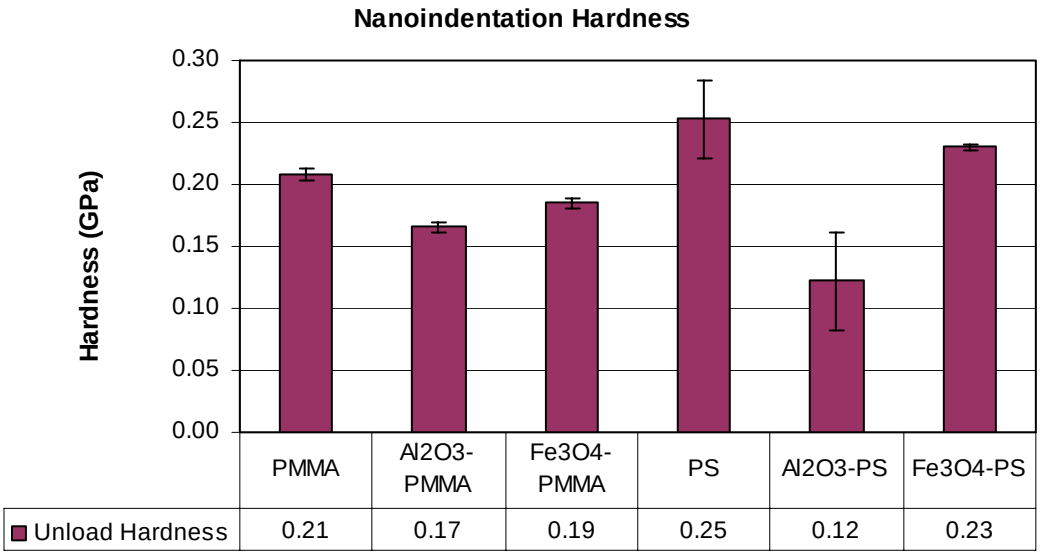

Figure 25. Nanoindentation unload hardness summary results.

Nanoparticle Dispersion

In polymer nanocomposites, many studies specify that good particle dispersion is critical to enable the most interaction with the polymer matrix and achieve the desired properties of the material.[5, 6, 8, 17, 25, 34] Both TEM and SEM were employed to evaluate the particle dispersion in this study.

SEM

The primary goal of using SEM was to determine particle size for interphase analysis, and to determine particle dispersion. SEM images were taken of the dogbone fracture surfaces of all four polymer nanocomposite systems. The fracture surfaces were sputter coated with gold atoms prior to imaging to avoid charging, but that did not negatively affect the image quality. Figure 26 – Figure 29, in subsequent pages, provide

example images showing the dispersion of particles. Particle size was measured from these and other images, covered later in the interphase characterization section.

Generally, the particles were not consistently dispersed. Flocculants of varying sizes, some very large, were found at the fracture sites. Figure 26(a) provides a low magnification (7,000 X) view of the PMMA-Fe_3O_4 fracture surface. Many particles of varying sizes are visible, appearing as small bright dots, fairly well dispersed across the image. Figure 26(b), however, shows a different area of the sample at the same magnification, and very few particles are present most of which have flocculated into two larger clusters. For the PS-Fe_3O_4 system, Figure 27(a) provides a low magnification view of the PS-Fe_3O_4 fracture surface showing dispersed particles, but fewer particles than the PMMA-Fe_3O_4 surface. On closer inspection of one of the particles at 80,000 X magnification, as shown in Figure 27(b), it is clear that flocculation has occurred since the larger mass appears to be an assortment of the smaller particles retaining their individual structure. It is not clear whether the particles flocculated before or after interaction with the polymer, since the polymer layer on each smaller particle could be disguised by additional polymer coating or by the sputter coating. Figure 28(a) shows a very large flocculate in the fracture surface of PMMA-Al_2O_3. On higher magnification viewing in Figure 28(b), it is clear that the particles are primarily individual capped particles that have flocculated together.

It is unknown whether the particles flocculated immediately after being mixed and capped in the PMMA solution, or if flocculation occurred sometime during the multiple heating periods in preparation of the dogbone sample. The dogbone samples have a distinct physical and thermal history. While evaporating the solvent in the

vacuum oven, the samples often bubbled above the mold surface while at a raised temperature. After solvent was removed they were subjected to higher temperatures and physically compressed into the dogbone mold. Given that the matrix molecules themselves are moving during both of these heating processes, it would seem to provide ample opportunity for movement of particles within the matrix and a settling in the same area. A very similar mass of particles was found in PS-Al_2O_3, as shown in Figure 29(a). The higher magnification view shows very distinct separation between the particles in this mass, as shown in Figure 29(b). All images showed some level of flocculation, but of varying sizes. In the PS-Fe_3O_4 system (Figure 27) the flocculant is approximately 200 X 100 nm in size. But in the PMMA-Al_2O_3 (Figure 28) and PS-Al_2O_3 (Figure 29) systems flocculants were several microns in diameter.

The SEM images indicate that the particles are not evenly dispersed throughout the dogbone samples; areas with no visible particles were found in each sample. This uneven dispersion could explain some of the ultimate strain and stress results that conflicted with the similar study by Ash, et al. Given the extreme nature of the thermal and physical history of the dogbone samples, however, one cannot assume that the dispersion is the same in the thin film samples used for DMA and nanoindentation.

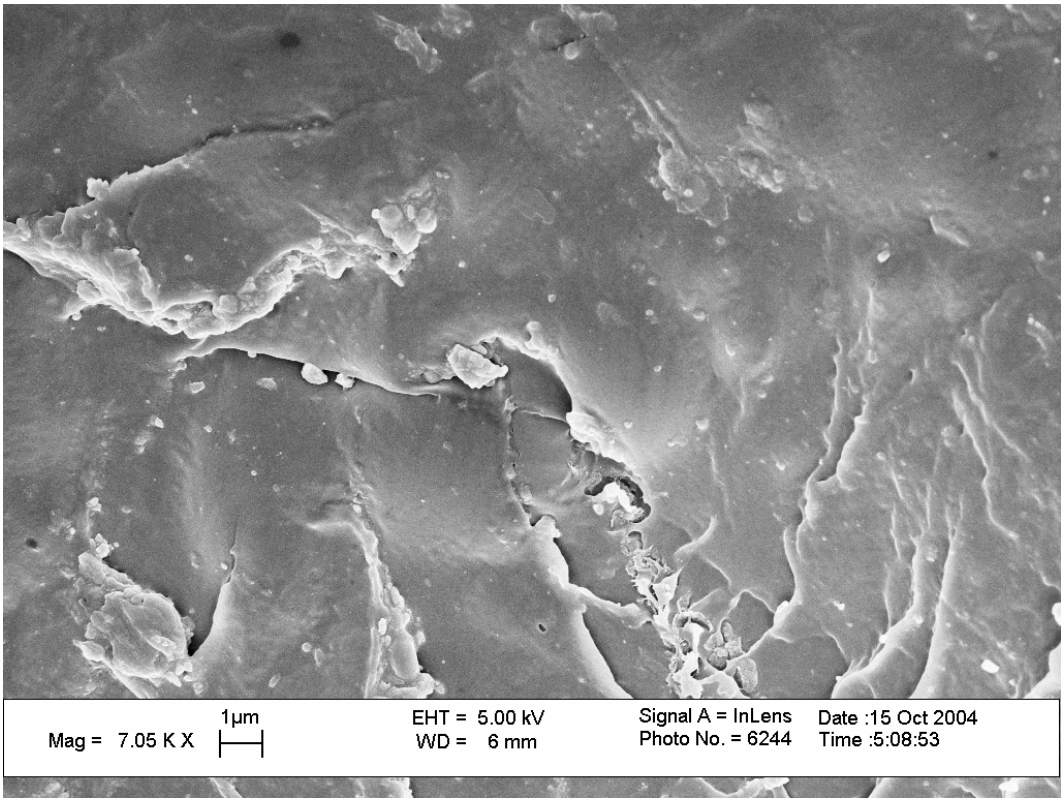

(a)

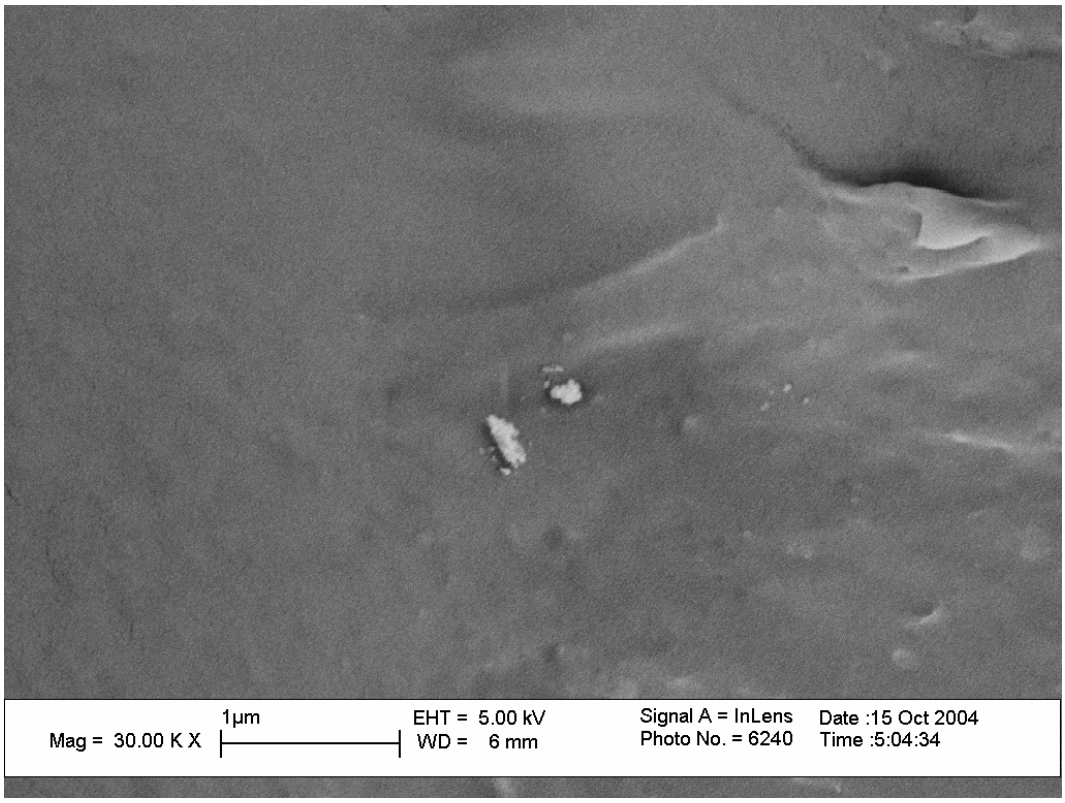

(b)

Figure 26. SEM images of PMMA-Fe_3O_4, (a) low magnification view of particle dispersion, (b) close-up view of a small flocculant.

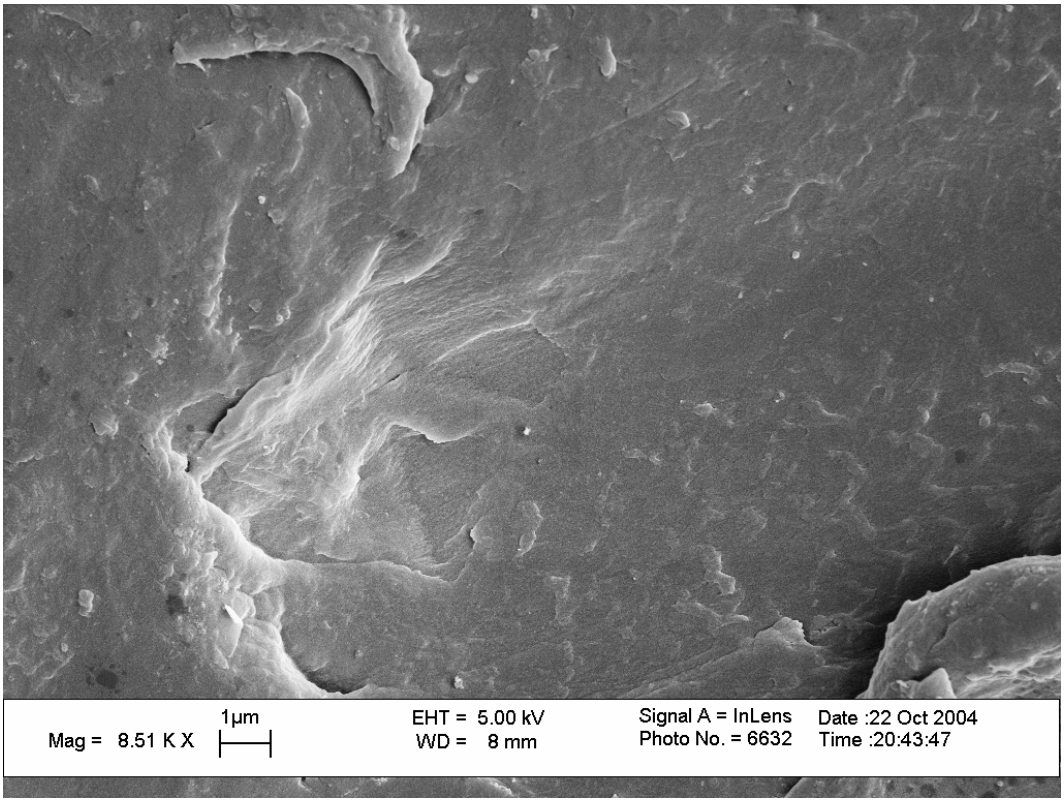

(a)

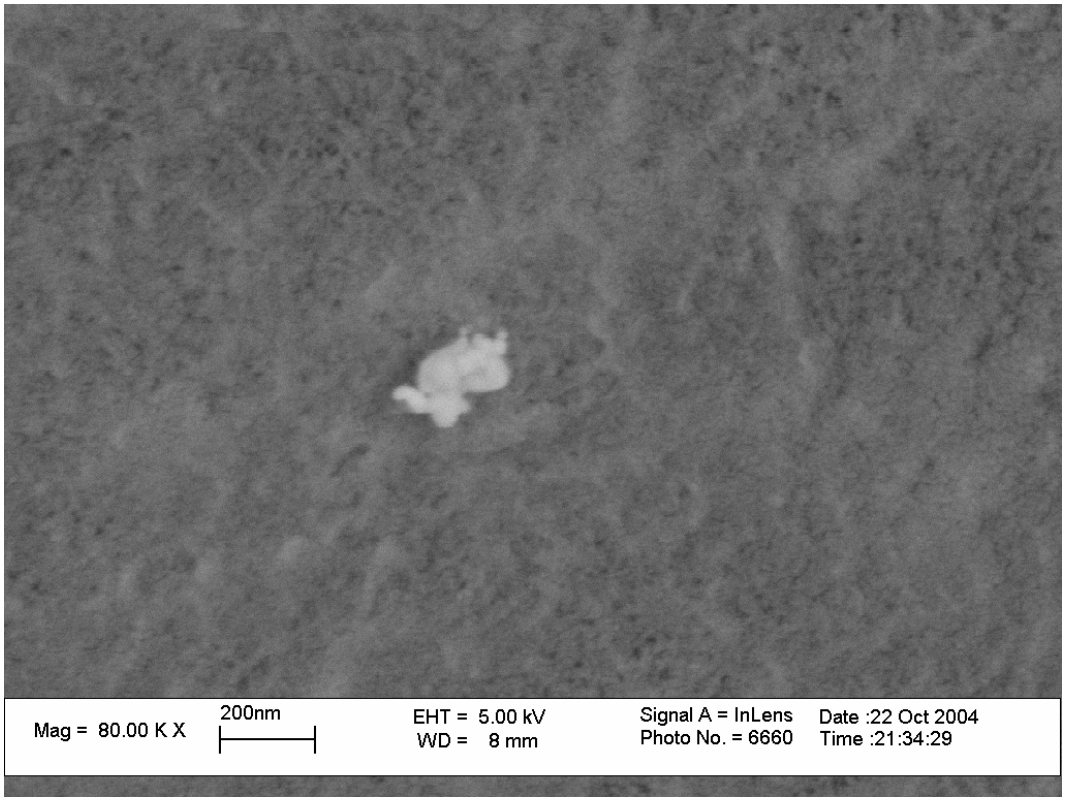

(b)

Figure 27. SEM images of PS-Fe_3O_4, (a) low magnification view of particle dispersion, b) close-up view of a small flocculant.

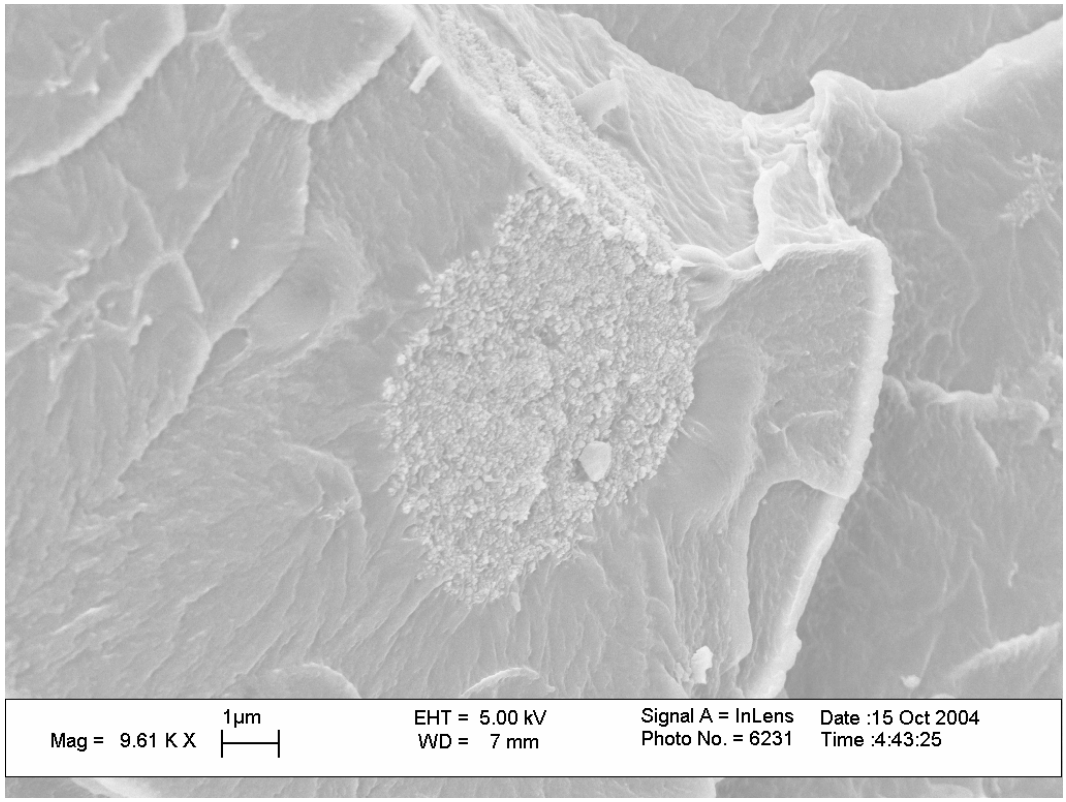

(a)

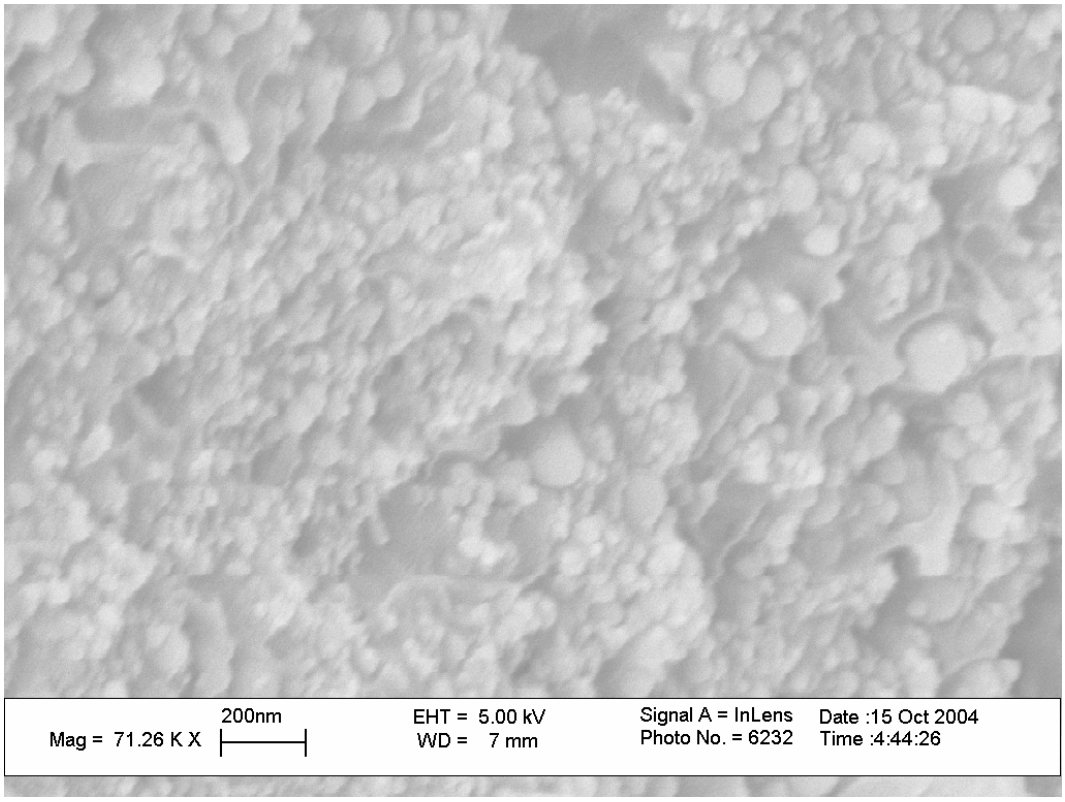

(b)

Figure 28. SEM images of PMMA-Al_2O_3, (a) low magnification view of a large flocculant, (b) close-up view of the particles within the flocculant.

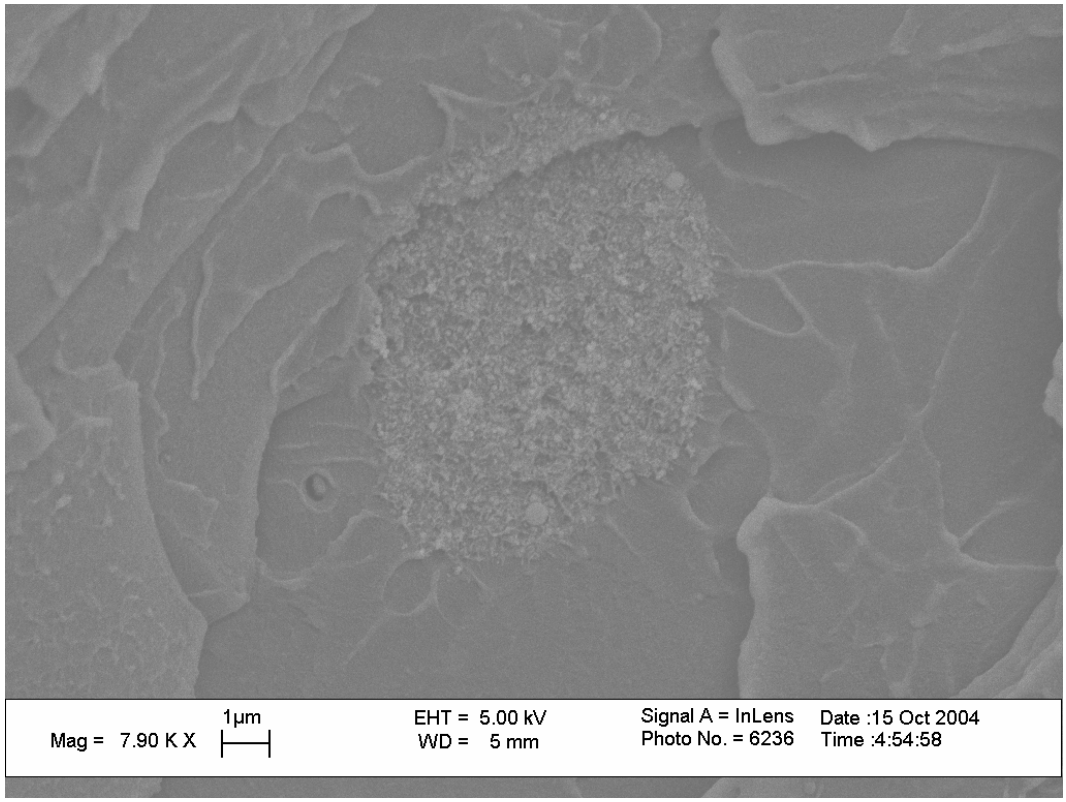

(a)

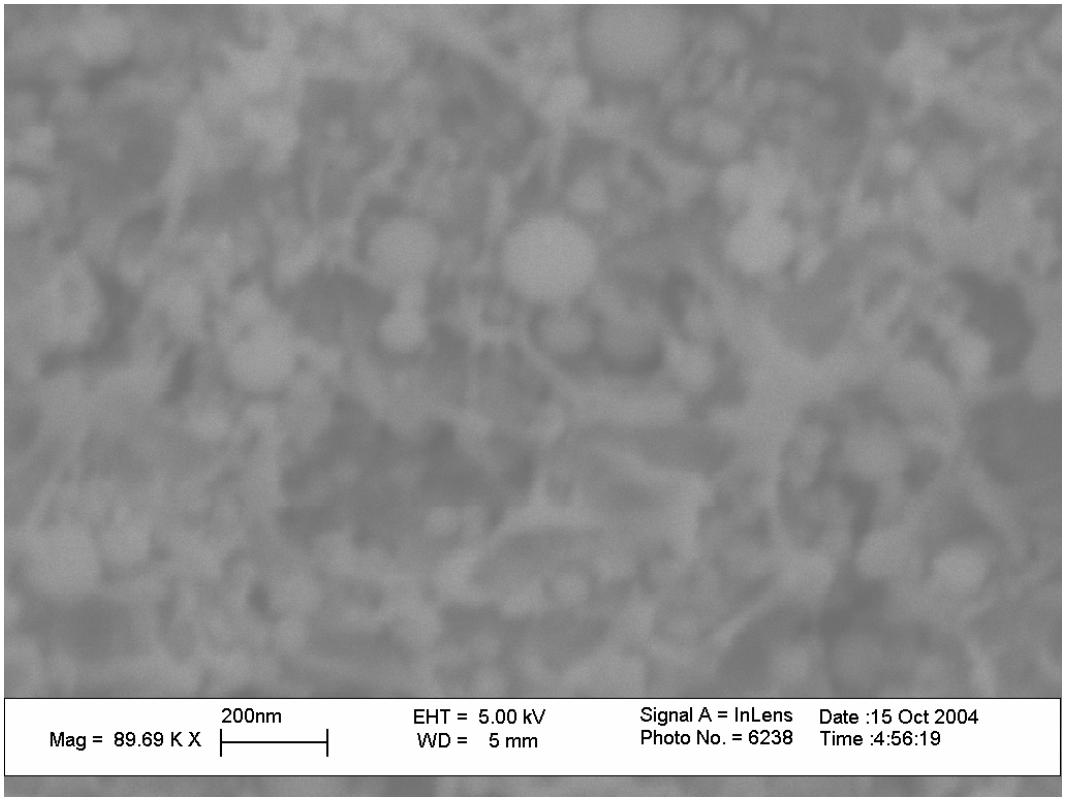

(b)

Figure 29. SEM images of PS-Al_2O_3, (a) low magnification view of particle dispersion, (b) close-up view of a small flocculant.

TEM

In previous studies TEM has been used to determine particle size and distribution. Likewise, the current study attempted to use TEM to image a diluted polymer nanocomposite solution. The optimal dilution that provides enough polymer to stabilize the particles in place but not too much or too thick to cloud TEM images, however, was not reached. Instead, polymer-capped particles, which were centrifuged from the polymer nanocomposite solution and washed to remove any non-bonded polymer, were imaged by suspending them in solvent and dripping the mixture over a TEM grid. Imaging capped particles does not provide any information regarding dispersion of nanoparticles in the matrix since they have been removed from matrix and re-suspended in solvent. The images, however, do provide information regarding likely sizes of particles present in the matrix. Figure 30 shows each of the polymer nanocomposite systems. The agglomeration of particles in the images is expected since the particles are suspended in solvent and they come together to lower their surface energy.

Particle sizes on the TEM images are worth noting. In Figure 30 (b) several Al_2O_3 particles in PS are ~40 nm, the size specified by the manufacturer, suggesting that a portion of the particles did not flocculate in the sample. In Figure 30(c), Fe_3O_4 in PMMA are as small as 10 nm, even though the manufacturer quotes average size of 90 nm. It is not clear whether the purchased nanoparticles had a wider size distribution, or processing broke apart and capped some of the particles into 10 nm particles.

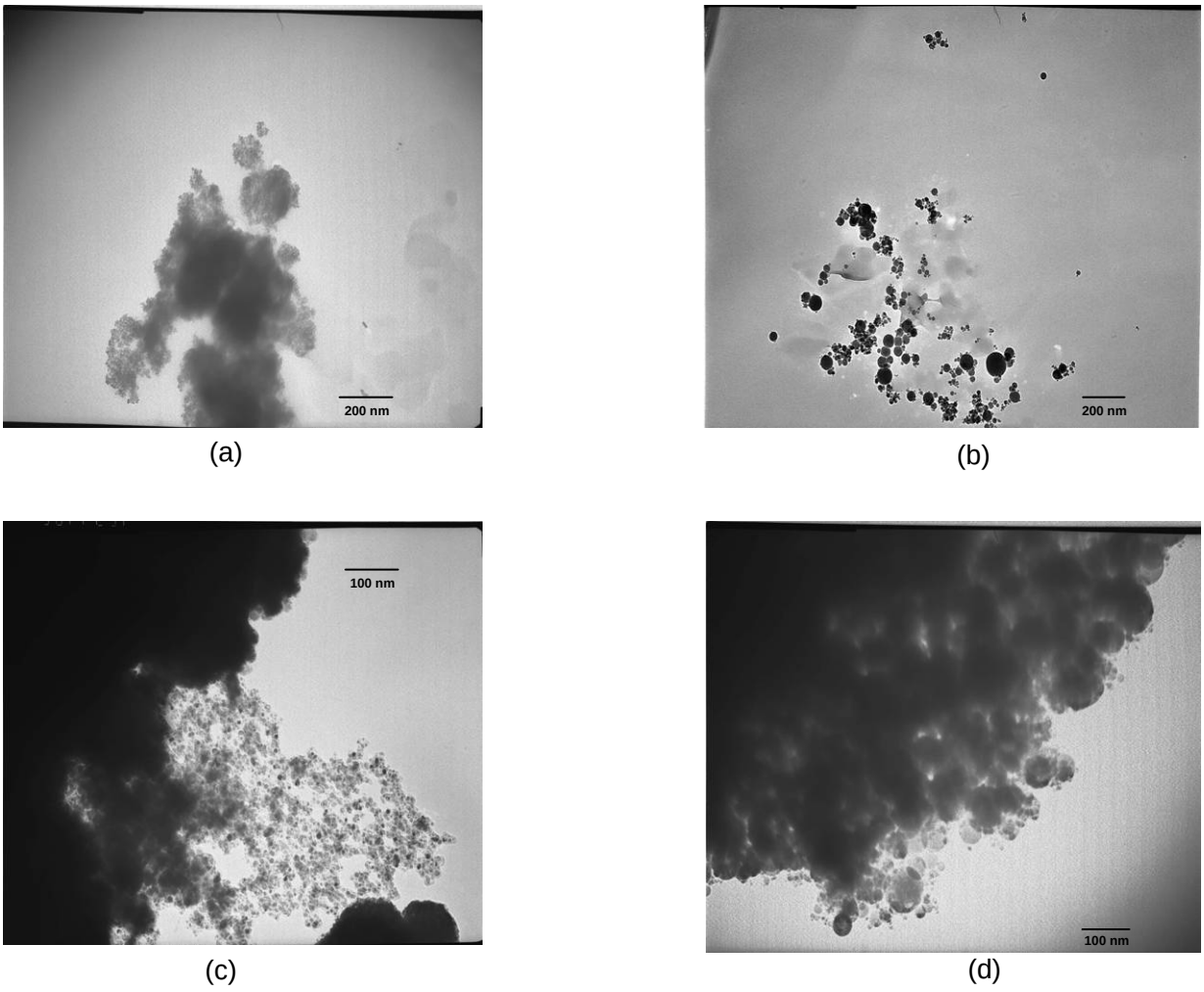

Figure 30. TEM image of polymer capped nanoparticle, (a) PS-Fe_3O_4, (b) PS-Al_2O_3, (c) PMMA-Fe_3O_4, (d) PMMA-Al_2O_3

Interphase Characterization

In an attempt to explain the mechanical testing results presented, the current study employed two approaches to characterize the interphase. Both approaches have been used in other research to characterize similar systems.[2, 39] In previous work, however, these results have not been combined with mechanical characterization of those same systems to determine the impact of the interphase properties. Although the different interphase characterization techniques take different approaches, they both assume that the structure of the interphase is a function of the nature of the interfacial interactions between the polymer and the reactive sites of the filler surface.[1] Both methods determine the average number of contact points between an adsorbed polymer chain and the nanoparticle. The number of contacts, or anchoring points, per chain indicates the density of polymer layer, and thus, the density of the interphase. A higher number of contact points per chain means the loops must be smaller so the entire adsorbed chain is closer to the surface and the interphase is denser.[1] This study attempted to find a relationship between the density of the interphase as described by these two approaches and the mechanical properties of the nanocomposites.

Interphase Characterization Using FT-IR

The first interphase characterization approach calculates the density of the interphase by investigating the bonding mechanism in the PMMA-based systems using FT-IR. The chemistry behind the interaction of PMMA and aluminum oxide surfaces is

well established.[39] The bonding process between the PMMA chain segments and the aluminum oxide nanoparticle surface is as follows.

The aluminum oxide nanoparticle surface molecules react with atmospheric water vapor creating oxyhydroxide surface groups:

$$Al_2O_3 + H_2O \rightleftharpoons 2AlO(OH) \tag{2}$$

This hydration reaction has been proven to occur with several metal oxides, including Al, Cr, Co, and Cu.[39] The presence of the OH group on the nanoparticle surface facilitates hydrolysis of the PMMA ester group to produce either a COOH acid group or its conjugate COO- base group, according to the following reaction:[39]

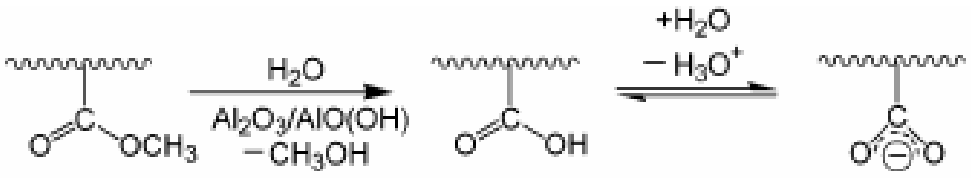

(3)

The COO- group directly interacts with the positively charged Al atoms to generate a bond between the polymer segment and the aluminum oxide nanoparticle surface.[27, 39] This bonded segment is an anchoring point for the PMMA chain.

FT-IR was performed on the PMMA-capped Fe_3O_4 and Al_2O_3 nanoparticles to confirm the interaction of the PMMA segments with the nanoparticles. The goal was to confirm that bonding occurs as described above, and to translate that bonding into interphase structure. Other work has shown that specific peaks in the IR spectrum indicate the existence of such bonding between PMMA and a metal oxide surface.[39]

Table 4 shows the peak ranges and specific bonds indicated by the peaks previously found.

Table 4. Infrared absorption bands of PMMA segment adsorption on Al_2O_3 surfaces.[39]

Peak	Indicator	Peak Assignment
2850-3050	Lower absorbance	O—CH_3 bond is broken
1730	Lower absorbance	C==O is no longer isolated
1685	Peak height	COO- group concentration
1140-1180	Inverse peak ratios	C—C and C—O stretching modes

FT-IR spectra for the two PMMA systems were examined for these particular bands. Figure 31 – Figure 33 show the relevant portions of the IR spectra for the PMMA-capped Fe_3O_4 and Al_2O_3 nanoparticles in a solution of chlorobenzene. By comparing these spectra to known spectra for PMMA dissolved in chlorobenzene, the bands indicating particle-polymer bonding are readily apparent. Interestingly, the Fe_3O_4 and Al_2O_3 spectra are nearly identical in absorbance along the entire spectrum.

(a)

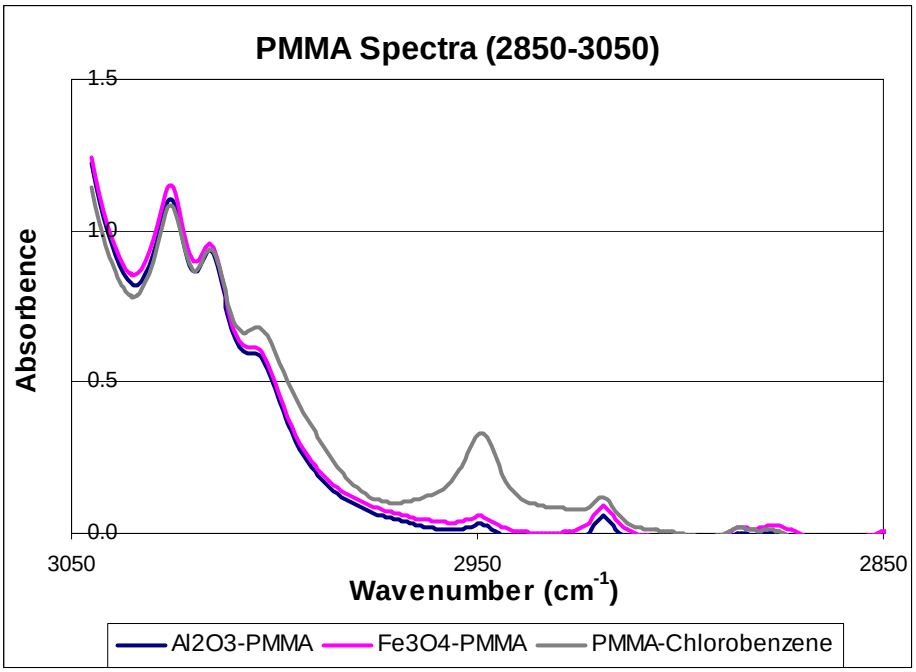

(b)

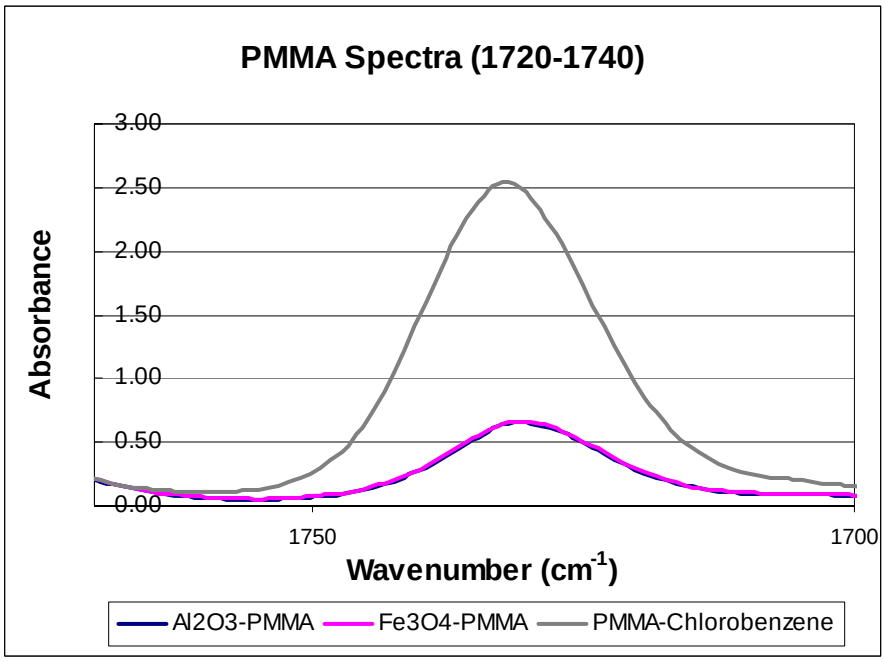

Figure 31. FT-IR spectra for PMMA-Fe_3O_4, PMMA-Al_2O_3, a PMMA-chlorobenzene systems showing the peak indicators for (a) the 2950 band indicating broken O—CH_3 and (b) the 1730 band indicating C==O is no longer isolated in some PMMA segments.

Figure 31Figure 31(a) indicates the lower absorbance of the 2950 peak for PMMA adsorbed on both Al_2O_3 and Fe_3O_4 particles. The lower absorbance indicates the first step in reaction (3), the detachment of the methyl group. The lower absorbance of the 1730 peak as compared to the PMMA/chlorobenzene spectra in Figure 31(b) indicates that some C==O bonds in the ester groups are no longer isolated, that is, they have been hydrolyzed to form the carboxylic acid (COOH) and carboxylic base (COO-) groups, the second and third steps of reaction (3).

The existence of these two peaks and indicators confirm the predicted bonding process between PMMA and aluminum oxide. Although Tannenbaum, et al. identified the reaction process and peak assignment for PMMA adsorption to an aluminum oxide particle surface, the similarity between the PMMA-Al_2O_3 and PMMA-Fe_3O_4 spectra suggests the adhesion mechanism for PMMA on magnetite nanoparticles is quite similar.

Since the PMMA segment's carboxylic base (COO-) participates in the bonding to the particle surface, quantifying the number of participating groups can serve as an estimate for the number of bonds. The 1685 cm^{-1} absorption band, shown in Figure 32, corresponds to the asymmetric stretch of the COO- group, which is indicative of the COO- group bonding with the surface.[39] Evaluating the ratio of the COO- groups participating in bonding (1685 absorbance) to the ester groups that are no longer isolated (1730 absorbance) provides the concentration of the COO- group. Using the peak height tool within the FT-IR computer software, the height of 1685 and 1730 peaks for PMMA-Al_2O_3 and PMMA-Fe_3O_4 were measured against baselines established using the tool.[39]

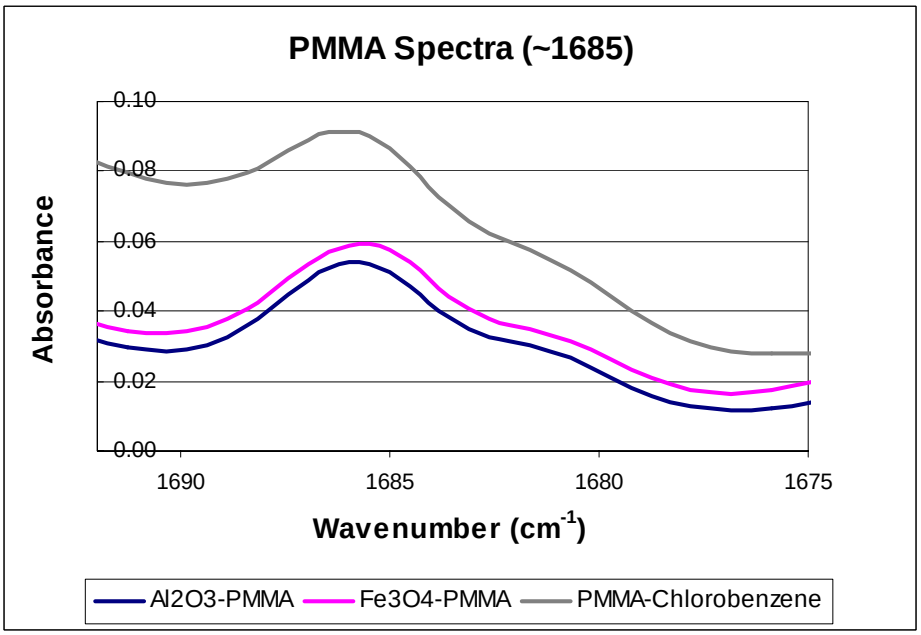

Figure 32. FT-IR spectra for PMMA-Fe_3O_4, PMMA-Al_2O_3, and PMMA-chlorobenzene systems showing 1685 cm^{-1} band indicating the absorbance of the carboxylic base (COO) groups.

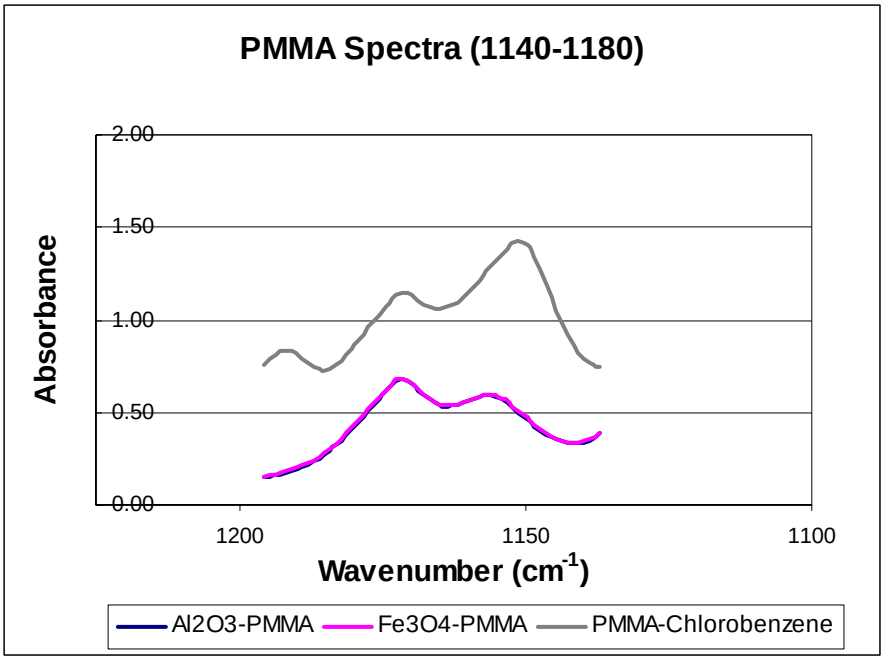

Figure 33. FT-IR spectra for PMMA-Fe_3O_4, PMMA-Al_2O_3, and PMMA-chlorobenzene systems showing the 1171 and 1151 cm^{-1} bands. Notice the shift in peak ratio between the chlorobenzene and the nanocomposite spectra.

The change in PMMA's configuration at the surface of a nanoparticle results in cooperative symmetric and antisymmetric stretches of the C—O and C—C groups. These configuration changes are represented by the changes in the relative intensities of the 1156 and 1171 infrared absorption bands. The shift in the relative intensity is very apparent when comparing the PMMA-chlorobenzene spectrum against the PMMA-capped nanoparticle spectra, as shown in Figure 33. The ratio of these two groups indicates the proportion of polymer segments that experience the configurational changes indicative of the bonding. The total number of PMMA carboxylate groups that have undergone hydrolysis and have anchored to the surface can be calculated from the ratio of the segments experiencing the configurational change and the concentration of the bonding group (COO). Multiplying this number by the average segment per polymer chain gives the number of anchoring points per chain, according to equation (4).[39]

$$\#\,Anchors/Chain = \frac{E_{1685}}{E_{1730}} \cdot \frac{E_{1156}}{E_{1171}} \cdot \frac{N_{monomers}}{N_{chains}} \qquad (4)$$

E_{1685} = absorbance intensity of the 1685 cm^{-1} infrared absorption band
E_{1730} = absorbance intensity of the 1730 cm^{-1} infrared absorption band
E_{1156} = absorbance intensity of the 1156 cm^{-1} infrared absorption band
E_{1171} = absorbance intensity of the 1171 cm^{-1} infrared absorption band
$N_{monomers}$ = total number of carboxylate groups
N_{chains} = total number of chains in the sample

The total number of chains in the sample and the total number of carboxylate groups are calculated using equations (5) and (6), respectively.

$$N_{chains} = \frac{M_{sample} \cdot w_{polymer} \cdot N_A}{\bar{M}_W} \quad (5)$$

M_{sample} = mass of sample [g]

$w_{polymer}$ = mass fraction of polymer as determined from TGA data [%]

N_A = # of chains per mole (Avogadro's Number) [chains/mole]

$\bar{M}_W$ = weight average molecular weight of polymer [g/mole]

$$N_{monomers} = \frac{\bar{M}_W \cdot N_{chains}}{M_{W-monomer}}$$

$M_{W-monomer}$ = molecular weight of monomer [g/mole] (6)

Using the data from the FT-IR spectra and using equation (4), the number of anchors per chain were calculated for the PMMA-based nanocomposites, as shown in Table 5.

Table 5. Absorbances from FT-IR spectra and the calculated number of anchors per chain for PMMA-Al_2O_3 and PMMA-Fe_3O_4 systems.

	PMMA-Al_2O_3	**PMMA-Fe_3O_4**
E_{1156}	0.3106	0.3109
E_{1171}	0.4528	0.4502
E_{1685}	0.0315	0.0323
E_{1730}	0.5507	.5772
N_{chains}	5.31E+14	1.06E+15
$N_{monomers}$	1.85E+18	3.69E+18
# Anchors / Chain	**137.2**	**135.1**

Interpreting the Results

The results in Table 5 are somewhat surprising given the results of previous studies. Following the same characterization approach, Tannenbaum, et al. calculated that cobalt oxide nanoclusters formed in the presence of PMMA ($\bar{M}_W$ = 330,000) formed 855 anchoring points per chain.[1] The study calculated the number of anchors for several different molecular weights of PMMA, showing that with longer, more flexible chains, the energetic penalty for the loss of configurational entropy due to chain confinement on the surface decreases. The strong interaction of the polymer with the surface outweighs the entropic loss and the more flexible chains can form additional anchoring points with the surface.[1] One might, therefore, expect that with the 350,000 molecular weight PMMA in the current study the number of anchoring points would be even higher. The difference in reactivity between Co_2O_3 and Al_2O_3 could account for some, but likely not all, of the disparity in number of anchoring points.

One critical difference between the current study and the referenced study taking the same approach could account for the differences in the results. Tannenbaum, et al. created the Co_2O_3 nanoparticles in the presence of PMMA via decomposition of cobalt carbonyls. The PMMA chains served to cap the forming clusters by limiting the aggregation of the nanoparticles. The polymer chains were introduced when the nanoparticles were in a very reactive state in the decomposition process. These very reactive sites could have provided much greater opportunity for the PMMA chains to bond to the surface. The current study, on the other hand, utilized pre-formed nanoparticle clusters that had already been processed and limited to a particular size. The

surfaces of these particles are far less reactive and provide less energetic drive for bonding with PMMA.

Interphase Characterization Using TGA and SEM

The second characterization approach calculated the number of anchoring points using the average cluster size from SEM and the total mass of the polymer directly absorbed on the metal clusters from TGA. Using this information, the structure of the loops and chains can be defined to determine the number of anchoring points. As shown in Figure 34, the interphase boundary extending out from a particle surface is described by the thickness of the polymer layer directly adsorbed onto the particle, L_{eff}. Within the interphase region, the adsorbed polymer chains form loops and trains over the surface. Assuming that the configuration of the polymer in the loops is that of a random coil, it is possible to calculate the minimum number of segments present in a loop, n_{loop}, based on the number of segments n_{eff} in a random coil of length L_{eff}. The number of segments in a loop combined with the molecular weight of the polymer determines the number of anchoring points per chain. In the following sections, data from TGA and SEM are used, combined with the derivation of this model, to determine the number of anchoring points.

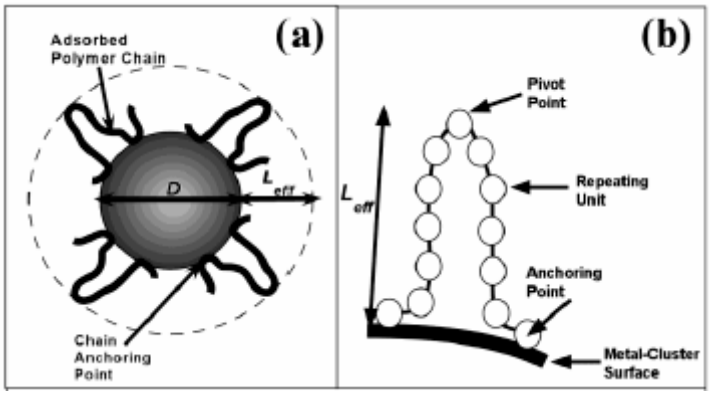

Figure 34. (a) Schematic description of the effective average polymer layer adsorbed on the nanoparticle, L_{eff} . (b) Schematic description of the actual number of free repeating units that exist in a polymer loop formed between two anchoring points, n_{loop} , and that are part of the chain that extends out and forms the thickness of the polymer layer.[39]

TGA Results

TGA decomposition data was obtained from capped particles to determine the weight fraction of the polymer layer adsorbed on the metal oxide particles. The difference between the starting and final weight of the sample represents the weight of the polymer burned off during the experiment. This weight fraction data enables calculation of the volume of the polymer around the particles. TGA experiments were run to a maximum temperature of 600˚C, well above the decomposition temperature of both PMMA and PS, but well below the decomposition temperatures of the metal oxides, to ensure that the polymer layer comprised the entire weight difference.

As seen in the PMMA-based system experiments, shown in Figure 35, the polymer layer comprised 9.1% of the PMMA-Al_2O_3 particles and 15.1% of the PMMA-Fe_3O_4 particles. Based only on this data, one might conclude that the Fe_3O_4 surfaces are more reactive with PMMA since more chains anchored to the surface. One important

consideration, however, is that more tightly bound chains can shield the surface from other chains likely resulting in fewer but more tightly bound chains.[1, 2] Therefore, this higher weight fraction of bound chains on Fe_3O_4 is likely due to weaker bonding of a higher number of chains with the surface.

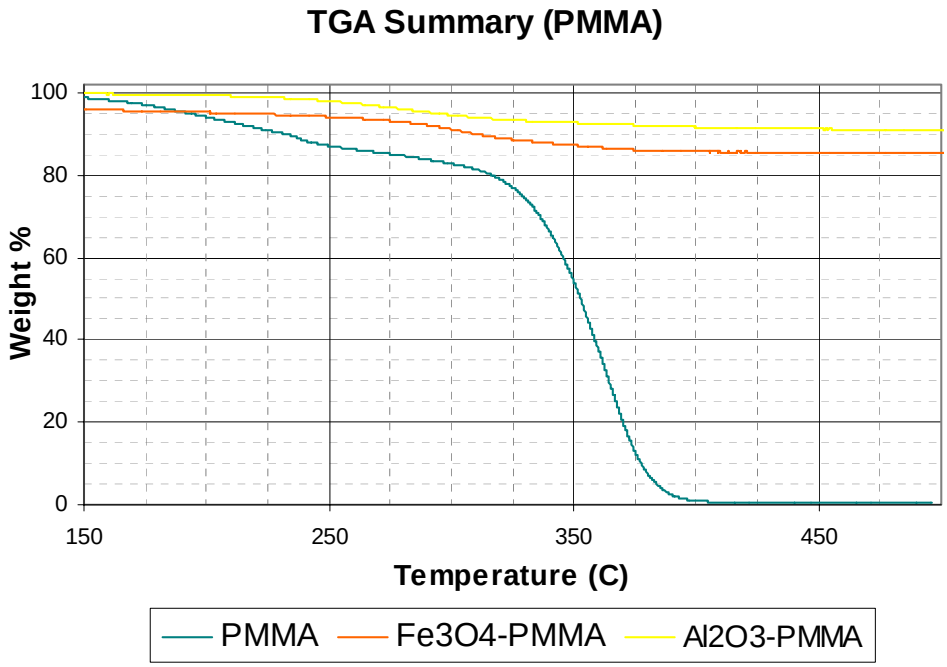

Figure 35. TGA decomposition data for the PMMA-based systems.

The PS-based systems, shown in Figure 36, provide similar results. The polymer weight fraction for PS-Fe_3O_4 was 11.9% and 9.6% for PS-Al_2O_3. Given the lower impact of configurational entropy loss because of the high molecular chains, the same conclusion regarding polymer bonding holds for the PS-based systems. PS is generally considered less reactive than PMMA,[1] but the data suggests that it is more reactive with the Al_2O_3 surfaces than with Fe_3O_4 surfaces, forming a denser layer.

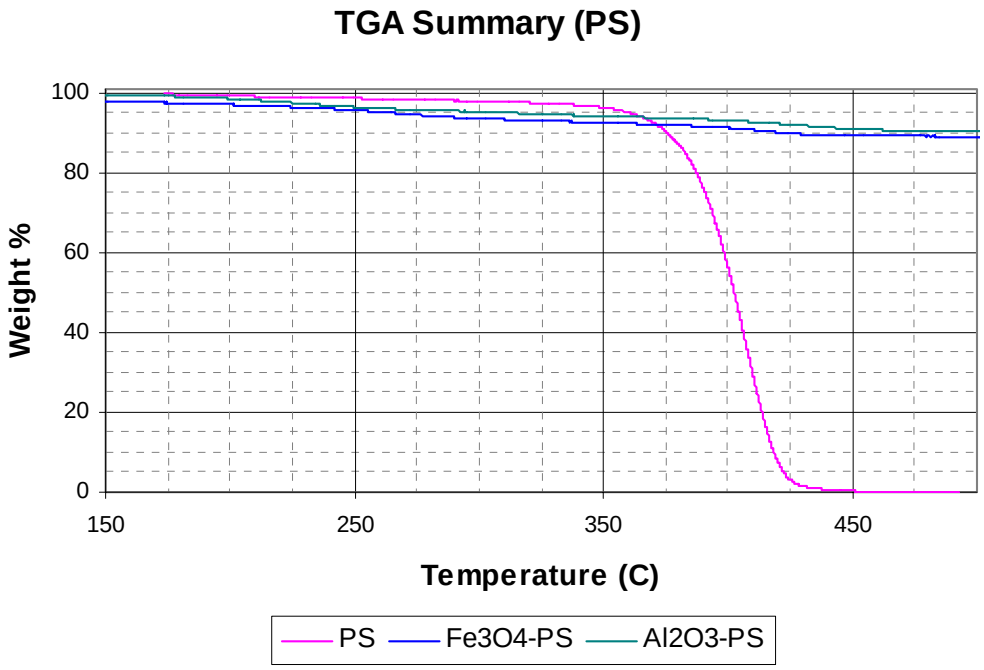

Figure 36. TGA decomposition data for the PS-based systems.

SEM Results (Particle Size)

SEM images of the dogbone fracture sites were analyzed to determine the average particle size in each nanocomposite system. The total particle size measured in SEM images includes both the diameter of metal oxide cluster and the thickness of the polymer layer bound to the surface of the cluster. By calculating the diameter of metal oxide clusters based on reference data and assumed geometry, one can solve for L_{eff}, which is a key component of this characterization approach. Several SEM images were taken of each sample, and all discernable particles on each image were measured. Note that even the distinct particles within the flocculants were measured individually because they

appeared to also be capped with a polymer layer. Figure 37 shows a sample of an SEM image from each system. Note that additional SEM images are provided in other parts of this paper.

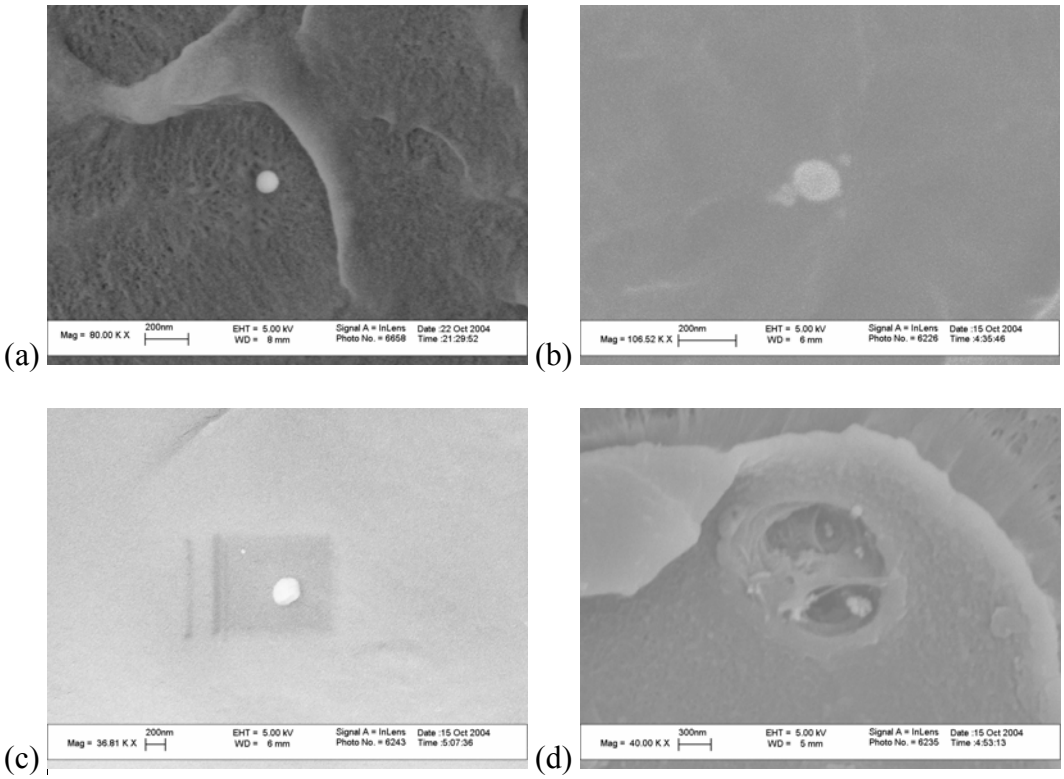

Figure 37. Sample SEM images of the dogbone fracture sites for (a) PS-Fe_3O_4, (b) PMMA-Al_2O_3, (c) PMMA-Fe_3O_4, and (d) PS-Al_2O_3. Images were used to measure particle diameter.

The number of particles measured for each sample across all images, the average particle size, and the standard deviation are presented in Table 6. The average particle size of 124-159 nm indicates flocculation has occurred among the particles. Within each polymer system it appears that Fe_3O_4 particles are slightly larger than the Al_2O_3 particles in the same polymer matrix. The difference in size between the two types of particles is understandable given that the starting average size specified by the manufacturer of the

Fe_3O_4 particles was 90 nm, compared to the Al_2O_3 starting size of 39 nm. However, any size related conclusion must be tempered by the very significant standard deviation in all systems. The large standard deviations indicate that there is a wide distribution of particle sizes in each system. In each system images show several particles existed with diameters well-below the starting particle size specified by the manufacturer of the particles. It is not clear whether the processing in the current study caused separation of clusters of particles or whether the manufacturer had more size variation than stated in the chemical specifications.

Table 6. Summary of average particle sizes as measured from SEM images.

	PMMA-Al_2O_3	**PMMA-Fe_3O_4**	**PS-Al_2O_3**	**PS-Fe_3O_4**
Number of particles	19	20	15	37
Diameter	124	139	135	154
Std Deviation	108	77	101	184

Interphase Calculations

With both the average particle size from SEM and the weight fraction of polymer in the capped-particle sample from TGA, the number of anchoring points per chain can be calculated. The first step is to derive the expression for the thickness of the bound polymer layer around the particles. The thickness of the polymer layer, L_{eff}, is determined by first considering the total volume of a polymer-capped particle, V_{total}. The total volume of the capped particle includes both the metal oxide cluster volume and the volume of the polymer layer bound to the surface.

$$V_{total} = V_{cluster} + V_{polymer} \tag{7}$$

The volume of the polymer adsorbed on the metal oxide cluster can be calculated using the weight fraction of the polymer, the mass of the TGA sample, and the number of clusters in the sample.

$$V_{polymer} = \frac{M_{sample} \cdot w_{polymer}}{N_{clusters} \cdot \rho} \tag{8}$$

M_{sample} = mass of the sample, as reported by TGA [g]
$w_{polymer}$ = mass fraction of polymer as determined from TGA data [%]
$N_{clusters}$ = average number of clusters in the sample
ρ = density of a thin film of polymer [g/nm^3]

Note that the density of PS is evaluated at 1.045 g/cm^3, or 1.05E-21 g/nm^3, and the density of PMMA is evaluated at 1.17E-21 g/nm^3. The number of clusters in the sample is the quotient of the number of molecules in the sample and the number of molecules per cluster.

$$N_{clusters} = \frac{N_{molecules}}{N_{molecule/cluster}} = \frac{\left(\frac{M_{sample} \cdot w_{cluster} \cdot N_A}{M_{W-molecule}} \right)}{\varepsilon \left(\frac{D_{cluster}}{d_{molecule}} \right)^3} \tag{9}$$

$N_{molecules}$ = total number of molecules in sample (eg Al_2O_3 molecules)
$N_{molecule/cluster}$ = number of molecules per cluster
$w_{cluster}$ = mass fraction of polymer after decomposition of the polymer as determined from TGA data [%]
N_A = # of chains per mole (Avogadro's Number) [chains/mole]
$M_{W-molecule}$ = molecular weight of one metal oxide molecule in cluster [g/mole]
$D_{cluster}$ = average diameter of clusters [nm]
$d_{molecule}$ = diameter of a molecule [nm]
ε = volume fraction of the molecules in the cluster, evaluated at 0.7.

The diameter of a molecule was calculated based on the manufacture-provided density of each metal oxide molecule.

$$atoms / nm^3 = \frac{N_A \cdot \rho_{molecule}}{M_{W-molecule}} \tag{10}$$

$\rho_{molecule}$ = density of molecule [g/nm^3]

Inverting equation (7) provides volume of a single atom.

$$nm^3 / atom = \frac{M_{W-molecule}}{N_A \cdot \rho_{molecule}} \tag{11}$$

The volume of a spherical atom can be expressed as $\frac{4\pi}{3} r^3$, so one can solve for r and attain the diameter of the atom.

c

$$r = \left(\frac{3M_{W-molecule}}{4\pi \cdot N_A \cdot \rho_{molecule}} \right)^{1/3} \tag{12}$$

$$d_{molecule} = 2 \times r \tag{13}$$

Using expression (9), the diameter of a Fe_3O_4 molecule is 0.52 nm and a Al_2O_3 molecule is 0.43 nm.

Assuming the clusters are geometrically spherical, the volume of a metal oxide cluster without an adsorbed polymer layer is

$$V_{cluster} = \left(\frac{4\pi}{3} \right) \left(\frac{D}{2} \right)^3 \tag{14}$$

$D_{cluster}$ = average diameter of clusters [nm]

The polymer capping layer adds a layer of thickness L_{eff} to each side of the diameter measurement, $D + 2L_{eff}$, so the total cluster volume with the adsorbed polymer layer is

$$V_{total} = \left(\frac{4\pi}{3}\right)\left(\frac{D + 2L_{eff}}{2}\right)^3 \tag{15}$$

With these two expressions for V_{total} we can derive an expression for L_{eff}. First, equation (14) is rearranged in terms of L_{eff}:

$$L_{eff} = \left(\frac{3}{4\pi}V_{total}\right)^{1/3} - \frac{D}{2} \tag{16}$$

Substituting expression (4) for V_{total} and simplifying through several steps leads an expression for L_{eff} that incorporates the TGA and SEM experimental data, as shown in expression (21).[20]

$$L_{eff} = \left(\frac{3}{4\pi}\left(V_{clusters} + V_{polymer}\right)\right)^{1/3} - \frac{D}{2} \tag{17}$$

$$L_{eff} = \left(\frac{3}{4\pi}\left(\left(\frac{4\pi}{3}\right)\left(\frac{D}{2}\right)^3 + \frac{M_{sample} \cdot w_{polymer}}{N_{clusters} \cdot \rho}\right)\right)^{1/3} - \frac{D}{2} \tag{18}$$

$$L_{eff} = \left(\left(\frac{D}{2}\right)^3 + \frac{3}{4\pi}\frac{M_{sample} \cdot w_{polymer}}{N_{clusters} \cdot \rho}\right)^{1/3} - \frac{D}{2} \tag{19}$$

$$L_{eff} = \left(\left(\frac{D}{2} \right)^3 + \frac{3}{4\pi} \frac{w_{polymer} \cdot M_{W-molecule} \cdot \varepsilon}{w_{cluster} \cdot N_A \cdot \rho} \left(\frac{D_{cluster}}{d_{molecule}} \right)^3 \right)^{1/3} - \frac{D}{2} \tag{20}$$

$$L_{eff} = \frac{1}{2} \left[\frac{6 w_{polymer} M_{W-molecule} \varepsilon}{\pi \rho w_{cluster} N_A} \left(\frac{D}{d_{molecule}} \right)^3 + D^3 \right]^{1/3} - \frac{D}{2} \tag{21}$$

Using expression (21) as the definition of L_{eff}, equation (22) calculates the average number of repeating units, n_{eff}, in a particular average chain length.

$$n_{eff} = \frac{1 + \cos\theta}{2(1 - \cos\theta)} \left(\frac{L_{eff}}{\sigma \cdot l} \right)^2 \tag{22}$$

θ = rotation angle for C-C bonds (109.5° for PS and PMMA)
σ = steric hindrance factor (2.3 for polystyrene and 2.1 for PMMA at room temperature)[53]
l = C-C bond length of 1.54 Å.

As shown in Figure 2 each side of a loop is made of repeating units, so the number of free repeating units that exist between two anchoring points, n_{loop}, is given by

$$n_{loop} = 2 \cdot n_{eff} - 1 \tag{23}$$

With these expressions, the number of anchoring points per chain can be calculated.

$$\#\,Anchors / Chain = \frac{N_{segments}}{n_{loop}} = \frac{\bar{M}_w}{M_{W-monomer} \left(2n_{eff} - 1 \right)} \tag{24}$$

$N_{segments}$ = average segments in chain
n_{loop} = the minimum number of segments present in a loop
$\bar{M}_W$ = weight average molecular weight of polymer [g/mole]
$M_{W-monomer}$ = molecular weight of monomer [g/mole]

n_{eff} = number of segments in random coil

$M_{W-monomer}$ = molecular weight of monomer [g/mole]

Using the data gleaned from the TGA and SEM and using equations (21-24), the number of anchoring points per chain were calculated for all four nanocomposite systems, as shown in Table 7.

Table 7. Calculation of interphase density using TGA and SEM experimental data.

	PMMA-Al_2O_3	**PMMA-Fe_3O_4**	**PS-Al_2O_3**	**PS-Fe_3O_4**
D [nm]	124	139	135	154
L_{eff} [nm]	4.59	10.92	5.87	9.47
n_{eff}	50.28	284.80	68.59	178.49
n_{loop}	99.55	568.60	136.18	355.98
# Anchors/Chain	**35.12**	**6.15**	**49.72**	**9.44**

Interpreting the Results

The results in Table 7 can be interpreted in a number of ways. Generally, PMMA is considered more reactive than PS,[5] and Al_2O_3 is more reactive than Fe_3O_4. These assumptions can be used to explain some of the results. For example, within the PS-based systems, PS-Al_2O_3 forms a much denser interphase (49.72 anchors/chain) than PS-Fe_3O_4 (9.44 anchors/chain), supporting the proposition that Al_2O_3 is more reactive than Fe_3O_4 with the polymer chains. Likewise for the PMMA-based systems, PMMA-Al_2O_3 forms a much denser interphase (35.12 anchors per chain) than PMMA-Fe_3O_4 (6.15 anchors per chain). These assumptions, however, do not apply as well to explaining the relative reactivity and interphase densities of a metal oxide across the PMMA and PS composite systems. While one would expect PMMA-Fe_3O_4 to form a denser interphase

than PS-Fe_3O_4 based on the relative reactivity of PMMA and PS, the results show the opposite effect. PMMA-Fe_3O_4 forms 6.15 anchors per chain while PS-Fe_3O_4 forms 9.44 anchors per chain, suggesting that PS is more reactive than PMMA with Fe_3O_4. PMMA-Al_2O_3 is similarly not in line with expectations as it forms 35.12 anchors per chain, while PS-Al_2O_3 forms 49.72 anchors per chain. Although these results are not consistent based on relative reactivity assumptions, the difference in results for the metal oxides across polymer systems is not significant.

Some of the calculations are consistent with previous research. Following the same characterization approach, Tannenbaum, et al. calculated that the number of anchors per chain of PS ($\bar{M}_w$=250,000) on Co_2O_3 nanoclusters was 52.9.[1] The current study's PS-Al_2O_3 ($\bar{M}_w$=350,000) results in Table 7 estimate 49.72 anchors per chain; these results are very similar. Other results, however, do not compare well to previous work. As stated earlier, Tannenbaum, et al. calculated that Co_2O_3 nanoclusters formed in the presence of PMMA ($\bar{M}_W$ = 330,000) formed 855 anchoring points per chain,[1] following the FT-IR characterization approach. Table 7 shows that the 35.12 anchors per chain for PMMA-Al_2O_3 is an order of magnitude different than Tannenbaum, et al.'s results of 855 anchors per chain. The same explanation of processing and lower particle reactivity, explained in the FT-IR approach section, holds for this interphase characterization approach. The much lower reactivity of the nanoparticles used in this study would likely result in less dense interphase with the matrix.

The huge standard deviation in nanoparticle size injects uncertainty into the results. The particle size is a critical variable in this characterization approach and the wide distribution of particle size suggests that the relatively small difference in values in

Table 7 means that detailed analysis is not conclusive. For example, the particle size provided in Table 7 for PMMA-Al_2O_3 is 124 with a standard variation of 108. The maximum and minimum particle sizes found in the images were 232 nm and 39 nm respectively. To get a sense of the dependence of the number of anchors per chain on particle size, if 232 nm were used as the particle diameter, this characterization approach predicts PMMA-Al_2O_3 would have 9.9 anchors per chain. If 39 nm is used, it would have 390.8 anchors per chain.

An interesting conclusion can be drawn when comparing the results for the two systems, PMMA-Al_2O_3 and PMMA-Fe_3O_4, for which both interphase characterization techniques provide results. As shown in Table 5, the FT-IR approach estimates 137.6 and 135.1 anchors per chain for PMMA-Al_2O_3 and PMMA-Fe_3O_4, respectively. As shown in Table 7MA-Al_2O_3 and PMMA-Fe_3O_4, respectively. As shown in Table 7, the TGA and SEM approach estimates 35.12 and 6.15 anchors per chain for PMMA-Al_2O_3 and PMMA-Fe_3O_4. Even though the results of the two approaches are not consistent, it is useful to use this TGA and SEM approach to check the results of the FT-IR approach. In order to force the TGA and SEM results to match the FT-IR results, the particle size can be adjusted. The TGA and SEM characterization matches the results of the FT-IR approach when the particle size for PMMA-Al_2O_3 is set to 64 nm, and PMMA-Fe_3O_4 is set to 39 nm. These particle sizes are not significantly different than the measured particle sizes including standard deviation.

Given the reasonable nature of the particle sizes required to synchronize the results, one could assume the particles are actually smaller than shown by SEM and the FT-IR approach could be giving the correct interphase density predictions. One must

keep in mind that the TGA and SEM approach only measured the particles at the fracture surface, while the FT-IR approach analyzed particles that could have existed anywhere in the dogbone sample. It is possible that the larger particles are on the fracture surface while the majority of the particles within the sample are smaller.

CHAPTER V

CONCLUSIONS

The polymer nanocomposite systems in this study, PMMA-Al_2O_3, PMMA-Fe_3O_4, PS-Al_2O_3, and PS-Fe_3O_4, do not provide improved mechanical properties over pure PMMA and PS systems. A decrease in elastic modulus for each system was proven with consistent results from tensile testing, DMA, and nanoindentation. Other mechanical properties of the four nanocomposite systems, including loss modulus and unload hardness, consistently decreased relative to the pure polymer systems.

Interphase characterization showed limited interaction between the Al_2O_3 and Fe_3O_4 nanoparticles with either of the polymer matrices, as compared to other studies of similar systems. The low number of anchoring points of polymer chains on the metal oxide surfaces calculated in this study results in a low density interphase in each of the nanocomposite systems. The low density interphase around the high number of nanoparticles results in the decrease of elastic modulus.

The simple mixing of pre-formed nanoparticles with polymer solution was not effective for good dispersion or size distribution. The approach does not benefit from polymer interaction with high-energy forming nanoparticles, as was experienced in other studies. Significant flocculation was observed in the fracture sites of the dogbone samples, indicating poor dispersion.

FT-IR analysis indicates significant similarities between the interaction of Al_2O_3 and Fe_3O_4 nanoparticles with PMMA. The two interphase characterization approaches,

however, did not provide consistent results. Factors contributing to the inconsistencies likely include wide particle size distribution, flocculation, and lower nanoparticle reactivity.

CHAPTER VI

RECOMMENDATIONS

Sample preparation methods must be improved in order to achieve good particle size distribution and dispersion. Any new approach must also enable production of enough well dispersed nanocomposite material to create the bulk samples for mechanical testing. The method of making dogbone samples should be improved to speed sample preparation and to achieve higher proportion of usable samples. An approach taken by other studies breaks apart thin sheets of hardened composite and places them into the dogbone molds for compression molding. The thin sheets could aid in solvent removal and shorten the preparation process. The molds used to make the dogbone samples should be recast with a more precise specification so solution does not leak from edges.

Utilizing different sizes of particles, including micro-sized particles would provide insight into the impact along a size spectrum. Varied concentrations of nanoparticles should be tested to understand the impact of concentration on properties. Other studies used a range of concentrations and suggested higher impact on mechanical properties with increased concentration. The 5% volume fraction used in this study should be the low starting point of further study, since some other studies use 5% weight fraction as their starting point, which is more concentrated than 5% volume fraction.

The interphase characterization approaches utilized in this study should be enhanced to deal with variables such as flocculation or varied filler geometries.

Microtomy should be employed to obtain thin slices of the bulk samples for use in determining size and distribution of particles, as opposed to obtaining data only from the fracture surface using with SEM. Thermal characterization using differential scanning calorimetry (DSC) of the different samples would assist in analyzing the interaction between the filler and matrix. Performing failure analysis on the fracture sites of dogbone samples of nanocomposites, microcomposites, and pure samples would help explain the mechanics of failure in nanocomposites. Other studies have indicated a distinct difference in the failure mechanism of their samples and further analysis could aid in improving mechanical properties.

ENDNOTES

1. Tannenbaum, R., Zubris, M. David, K., Jacob, K., Jasiuk, I., Dan, N., *Characterization of Metal-Polymer Interfaces in Nanocomposites and the Implications to Mechanical Properties*, Georgia Institute of Technology. p. 1-20.

2. Lipatov, Y.S., *Polymer Reinforcement*. 1995: ChemTec Publishing. 385.

3. Su, S., Jiang, D.D., Wilkie, C.A., *Methacrylate Modified Clays and Their Polystyrene and Poly(methyl methacrylate) Nanocomposites.* Poly. Adv. Technol., 2004. **15**: p. 225-231.

4. Gersappe, D., *Molecular Mechanisms of Failure in Polymer Nanocomposites.* Physical Review Letters, 2002. **89**(5): p. 058301-1-4.

5. Vollenberg, P.H.T., Heikens, D., *Particle Size Dependence of the Young's Modulus of Filled Polymers: 1. Preliminary Experiments.* Polymer, 1989. **30**(September): p. 1656-1662.

6. Chan, C.-M., Wu, J., Li, J.-X., Cheung, Y.-K., *Polypropylene/Calcium Carbonate Nanocomposites.* Polymer, 2002. **43**: p. 2981-2992.

7. Park, J.H., Jana, S.C., *The Relationship Between Nano- and Micro-Structures and Mechanical Properties in PMMA-Epoxy-Nanoclay Composites.* Polymer, 2003. **44**: p. 2091-2100.

8. Reynaud, E., Jouen, T., Gauthier, C., Vigier, G. Varlet, J., *Nanofillers in Polymeric Matrix: A Study on Silica Reinforced PA6.* Polymer, 2001. **42**: p. 8759-8768.

9. Wu, C.L., Zhang, M.Q., Rong, M.Z., Friedrich, K., *Tensile Performance Improvement of Low Nanoparticles Filled-Polypropylene Composites.* Composites Science and Technology, 2002. **62**: p. 1327-1340.

10. Shelley, J.S., Mather, P.T., DeVries, K.L., *Reinforcement and Environmental Degradation of Nylon-6/Clay Nanocomposites.* Polymer, 2001. **42**: p. 5849-5858.

11. Alexandre, M., Dubois, P., *Polymer-layered Silicate Nanocomposites: Preparation, Properties, and Uses of a New Class of Materials.* Material Science and Engineering, 2000. **28**: p. 1-63.

12. Rong, M.Z., Zhang, M.Q., Pan, S.L., Lehmann, B., Friedrich, K., *Analysis of the Interfacial Interactions in Polypropylene/Silica Nanocomposites.* Polymer International, 2003. **53**: p. 176-183.

13. Shang, S.W., Williams, J.W., Soderholm, K-J.M., *How the Work of Adhesion Affects the Mechanical Properties of Silica-Filled Polymer Composites.* 1994.

14. Brechet, Y., Cavaille, J.-Y. Y., Chabert, E., Chazeau, L., Dendievel, R., Flandin, L. Gauthier, C., *Polymer Based Nanocomposites: Effect of Filler-Filler and Filler-Matrix Interactions.* Advanced Engineering Materials, 2001. **3**(8): p. 571-577.

15. Jordan, J., Sharaf, M., Jacob, K., Tannenbaum, R., Jasiuk, I., *Experimental Trends in Polymer nanocomposites - A Review*, Georgia Institute of Technology. p. 1-29.

16. Zhu, L., Narh, K.A., *Numerical Simulation of the Tensile Modulus of Nanoclay-Filled Polymer Composites.* Journal of Polymer Science: Part B: Polymer Physics, 2004. **42**: p. 2391-2406.

17. Ash, B.J., Stone, J., Rogers, D.F., Schadler, L.S., Siegel, R.W., Benicewicz, B.C., Apple, T., *Investigation into the Thermal and Mechanical Behavior of PMMA/Alumina Nanocomposites*, in *Filled and Nanocomposite Polymer Materials*. 2001, Materials Research Society: Boston, MA. p. KK2.10.1-10.6.

18. Bolhuis, P.G., Louis, A.A., Hansen, J.-P., *Influence of Polymer Excluded Volume on the Phase Behavior of Colloid-Polymer Mixtures*. 2002, University of Amsterdam. p. 1-5.

19. Jancar, J., Dibenedetto, A.T., Dianselmo, A., *Effect of Adhesion of the Fracture toughness of Calcium Carbonate-Filled Polypropylene.* Polymer Engineering and Science, 1993. **v 33**(n 9): p. 559-563.

20. Tadd, E., Zeno, A. Zubris, M., Dan, N., Tannenbaum, R., *Adsorption and Polymer Film Formation on Metal Nanoclusters.* Macromolecules, 2003. **36**: p. 6497-6502.

21. Petrovic, Z.S., Javni, I., Wasson, A., Banhegyi, G., *Structure and Properties of Polyurethane-Silica Nanocomposites.* Journal of Applied Polymer Science, 2000. **76**: p. 133-151.

22. Kardos, J.L., *Role of the Interface in Polymer Composites - Some Myths, Mechanisms, and Modifications*, in *Polymer Preprints, Division of Polymer Chemistry, American Chemical Society: Papers Presented at the Seattle Meeting.* 1983, ACS, Div of Polymer Chemistry: Seattle, WA, USA.

23. Vollenberg, P.H.T., Heikens, D., *The Mechanical Properties of Chalk-Filled Polypropylene: A Preliminary Investigation.* 1990: p. 3089-3095.

24. Kovacevic, V., Lucic, S., Leskovac, M., *Morphology and Failure in Nanocomposites. Part I: Structural and mechanical Properties.* J. Adhesion Sci. Technol., 2002. **16**(10): p. 1343-1365.

25. Kovacevic, V., Leskovac, M., Lucic Blagojevic, S., *Morphology and Failure in Nanocomposites. Part II: Surface Investigation.* J. Adhesion Sci. Technol., 2002. **16**(14): p. 1915-1929.

26. Vollenberg, P.H.T., de Haan, J.W., van de Ven, L.J.M, Heikens, D., *Particle Size Dependence of the Young's Modulus of Filled Polymers: 2. Annealing and Solid-State Nuclear Magnetic Resonance Experiments.* Polymer, 1989. **30**(September): p. 1663-1668.

27. King, S., Hyunh, K., Tannenbaum, R., *Kinetics of Nucleation, Growth, and Stabilization of Cobalt Oxide Nanoclusters.* J. Phys. Chem. B, 2003. **107**: p. 12097-12104.

28. Fekete, E., Molnar, Sz., Kim, G.-M., Michler, G.H., Pukanszky, B., *Aggregation, Fracture Initiation, and Strength of PP/$CaCO_3$ Composites.* Journal of Macromolecular Science, 1999. **v B38**(n 5-6): p. 885-899.

29. Chabert, E., Gauthier, C., Dendievel, R., Chazeau, L., Cavaille, J.-Y. Y., *Mechanical Behavior of Polymer Nanocomposites: A Discrete Simulation Approach.* Mat. Res. Soc. Symp. Proc., 2003. **740**: p. 16.1.1-16.1.6.

30. Shia, D., Hui, C.Y., Burnside, S.D., Giannelis, E.P., *Interface Model for the Prediction of Young's Modulus of Layered Silicate-Elastomer Nanocomposites.* Polymer Composites, 1998. **19**(5): p. 608-617.

31. Nowicki, W., *Structure and Entropy of a Long Polymer Chain in the Presence of Nanoparticles.* Macromolecules, 2002. **35**: p. 1424-1436.

32. Skau, K.I., Blokhuis, E.M., *Polymer Adsorption on Curved Surfaces: Finite Chain Length Corrections.* Macromolecules, 2003. **36**: p. 4637-4645.

33. Aubouy, M., Raphael, E., *Scaling Description of a Colloidal Particle Clothed with Polymers.* Macromolecules, 1998. **31**: p. 4357-4363.

34. David, K., Dan, N., Tannenbaum, R., *Competitive Adsorption of Polymers on Metallic Nanoparticles*. 2004, Georgia Institute of Technology. p. 33.

35. Dan, N., *Effect of Polymer Adsorption on the Surface Tension and Flocculation of Colloidal Particles in Incompatible Solvents.* Langmuir, 2000. **16**: p. 4045-4048.

36. Ou, Y., Yang, F., and Yu, Z.-Z., *A new conception on the toughness of nylon 6/silica nanocomposite prepared via in situ polymerization.* Journal of Polymer Science: Part B: Polymer Physics, 1998. **36**: p. 789-795.

37. Yang, F., Ou, Y., and Yu, Z., *Polyamide 6/silica nanocomposites prepared by in situ polymerization.* Journal of Applied Polymer Science, 1998. **69**: p. 355-361.

38. Zeng, C., Lee, L. J., *Poly(methyl methacrylate) and Polystyrene/Clay Nanocomposites Prepared by in-Situ Polymerization.* Macromolecules, 2001. **34**: p. 4098-4103.

39. Tannenbaum, R., King, S., Lecy, J., Tirrell, M., Potts, L., *Infrared Study of the Kinetics and Mechanism of Adsorption of Acrylic Polymers on Alumina Surfaces.* Langmuir, 2004. **20**: p. 4507-4514.

40. Plastics Technology Laboratories, Inc., http://www.ptli.com/testlopedia/subs/DMA.asp

41. Al-Haik, M.S., Garmestani, H., Li, D.S., Hussaini, M.Y., Sablin, S.S., Tannenbaum, R., Dahmen, K., *Mechanical Properties of Magnetically Oriented Epoxy.* Journal of Polymer Science: Part B: Polymer Physics, 2004. **42**: p. 1586-1600.

42. VanLandingham, M.R., Villarrubia, J.S., Guthrie, W.F., Meyers, G.F., *Nanoindentation of Polymers: An Overview.* Macromolecules Symposium, 2001. **167**: p. 15-43.

43. Fischer-Cripps, A.C., *Nanoindentation*. Mechanical Engineering Series, ed. F.F. Ling. 2002, New York: Springer-Verlag. 194.

44. VanLandingham, M.R., *Review of Instrumented Indentation.* Journal of Research of the National Institute of Standards and Technology, 2003. **108**(4): p. 249-265.

45. Materials Evaluation and Engineering, Inc., Handbook of Analytical Methods for Materials, http://www.mee-inc.com/ham.html

46. Campbell, D., Pethrick, R.A., White, J.R., *Polymer characterization: physical techniques*, ed. S. Thornes. 2000, U.K.: Cheltenham. 481.

47. Goldstein, J.I., Newbury, D. E., Echlin, P., Joy, D.C., *Scanning Electron Microscopy and X-Ray Microanalysis*. 1992, New York: Plenum Press.

48. Szymanski, H.A., *IR: Theory and Practice of Infrared Spectroscopy*. 1964, New York: Plenum Press. 375.

49. Goodfellow Corporation, Polymer Properties Table, http://www.goodfellow.com/csp/active/gfMaterialTablesList.csp

50. Tuck, J.R., Korsunsky, A.M., Bull, S.J., Davidson, R.I, *On the Application of the Work-of-Indentation Approach to Depth-Sensing Indentation Experiments in Coated Systems.* Surface and Coatings Technology, 2000. **137**(n 2-3): p. 217-224.

51. Ishikawa, H., Fudetani, S., Hirohashi, M., *Mechanical Properties of Thin Films Measured by Nanoindenters.* Applied Surface Science, 2001. **178**: p. 56-62.

52. Rice, P.M., Stoller, R.E. *Correlation of Nanoindentation and Conventional Mechanical Property Measurements*. in *Materials Research Society Symposium - Proceedings*. 2000: Materials Research Society.

53. Young, R.J., Lovell, P. A., *Introduction to Polymers*. Second ed. 1991, London: Chapman & Hall. 443.